ERDA/JPL 954373—77/3
Distribution Category UC-63

HEAT EXCHANGER-INGOT CASTING/SLICING PROCESS

Silicon Sheet Growth Development for the Large Area Silicon Sheet Task of the Low Cost Silicon Solar Array Project

EIGHTH QUARTERLY PROGRESS REPORT

BY

FREDERICK SCHMID AND CHANDRA P. KHATTAK

Covering Period from July 1, 1977 to September 30, 1977

Date of Report: October 1, 1977

JPL Contract No. 954373

(NASA-CR-155717) HEAT EXCHANGER-INGOT CASTING/SLICING PROCESS: SILICON SHEET GROWTH DEVELOPMENT FOR THE LARGE AREA SILICON SHEET TASK OF THE LOW COST SILICON SOLAR ARRAY PROJECT Quarterly Progress N78-72735 Unclas 00/44 04174.

CRYSTAL SYSTEMS INC.

Shetland Industrial Park
P.O. Box 1057, Salem, Mass. 01970

REPRODUCED BY
NATIONAL TECHNICAL INFORMATION SERVICE
U.S. DEPARTMENT OF COMMERCE
SPRINGFIELD, VA. 22161

This work was performed for the Jet Propulsion Laboratory, California Institute of Technology, under NASA Contract NAS7-100 for the U.S. Energy Research and Development Administration, Division of Solar Energy.

The JPL Low-Cost Silicon Solar-Array Project is funded by ERDA and forms part of the ERDA Photovoltaic Conversion Program to initiate a major effort toward the development of low-cost solar arrays.

91

ERDA/JPL 954373 - 77/3
Distribution Category UC-63

HEAT EXCHANGER-INGOT CASTING/SLICING PROCESS

Silicon Sheet Growth Development for the
Large Area Silicon Sheet Task of the Low Cost
Silicon Solar Array Project

Eighth Quarterly Progress Report

by
Frederick Schmid and Chandra P. Khattak

Covering Period from July 1, 1977 to September 30, 1977
Date of Report: October 1, 1977

JPL Contract No. 954373

CRYSTAL SYSTEMS, INC.
35 Congress Street
P.O. Box 1057
Salem, MA 01970

This work was performed for the Jet Propulsion Laboratory, California Institute of Technology, under NASA Contract NAS7-100 for the U. S. Energy Research and Development Administration, Division of Solar Energy.

The JPL Low-Cost Silicon Solar Array Project is funded by ERDA and forms part of the ERDA Photovoltaic Conversion Program to initiate a major effort toward the development of low-cost solar arrays.

This report contains information prepared by Crystal Systems, Inc., under JPL subcontract. Its content is not necessarily endorsed by the Jet Propulsion Laboratory, California Institute of Technology, or the National Aeronautics and Space Administration, or the U. S. Energy Research and Development Administration, Division of Solar Energy.

MAN-HOURS AND COST TOTALS

Previous		Current		Cumulative	
M/Hr.	Cost	M/Hr.	Cost	M/Hr.	Cost
8,592	$383,340	2,111	$107,035	10,703	$490,375

TABLE OF CONTENTS

	Page
ABSTRACT	iv
SUMMARY AND PROGRESS	1
CRYSTAL CASTING	1
Crucible Development	2
Sources of Formation of Silicon Carbide - Theoretical	25
1. Introduction	25
2. Sources of Thermochemical Data Employed in the Analysis	25
3. Consideration of the Reaction between Liquid Silicon and Silica Crucible	27
4. Consideration of the Reaction between Liquid Silicon and Silica Crucible	27
5. Examination of the CO/CO_2 Equilibrium in the Working Range	29
6. Evaluation of the Reaction between Oxygen Dissolved in Silicon with Silicon to Form Gaseous SiO	31
7. Consideration of the Simultaneous Reaction of Carbon and Oxygen in Liquid Silicon	33
8. Detailed Calculation of the Rate of Evaporation of Silicon Monoxide	34
9. Comparison of the Calculated Rate with the Rate Observed During a Crystal Growth Experiment	35

CONTENTS (Cont.)

10. Consideration of Reactions between Graphite and Silica Crucible. 36

11. Consideration of Reaction between CO and C with SiO 40

12. Consideration of Reaction between CO or CO_2 with Silicon 42

Results. 47

Source of Formation of Silicon Carbide - Experimental 48

Efforts to Eliminate Silicon Carbide 49

Results. 57

Improvement of Heat Extraction through the Crucible. 58

CRYSTAL SLICING. 62

Wafer Surface Characterization 69

Blade Development 71

PROJECTED ADD-ON COST ANALYSIS FOR PRODUCING SILICON WAFERS 76

CONCLUSIONS 81

REFERENCES 83

MILESTONES 84

ABSTRACT

Graded crucibles have been developed which are dense enough to avoid penetration of the molten silicon and weak enough to fracture during the cool-down cycle. These crucibles have been used to cast crack-free silicon ingots up to 3.3 kg. Significant progress has been made in the crystallinity of the samples cast. Solar cells made from one of the ingots have yielded over 9% conversion efficiency.

The source of silicon carbide in the cast silicon has been identified, both theoretically and experimentally, to be associated with the use of graphite retainers in contact with the crucible.

Both 45 μm and 30 μm diamonds can be used for efficient slicing of silicon. Wafers sliced with 45 μm diamond plated wire show a surface roughness of ± 0.5 μm and extent of damage of 3 μm. In an effort to avoid diamond pullout from impregnated wire it was found that a layer of 0.3 mil thick plating is sufficient to encapsulate the diamonds.

A projected cost analysis has shown that the add-on cost of casting and slicing of silicon is $11.57 per square meter.

SUMMARY AND PROGRESS

CRYSTAL CASTING

Efforts during this quarter were directed towards establishing the proof of concept of the Heat Exchanger Method (HEM) to cast silicon. One of the major problems encountered was the cracking of ingot during the cool-down cycle. In this respect a crucible development effort was pursued to develop a suitable graded crucible which prevented the ingot from cracking. Large sound ingots, weighing up to 3.3 Kg, have been cast using such crucibles. This has, therefore, established the proof of concept of the process.

The ingots presently cast are expected to have a high impurity content. One of the sources of these impurities is the formation of silicon carbide. Efforts were made to understand the cause of silicon carbide formation, both from a theoretical as well as experimental point of view.

In order to achieve higher growth rates it is suggested to use a graphite plug through a hole at the bottom of the crucible. Experiments were carried out to achieve a seal between the graphite plug and silica crucible which is leakproof to

molten silicon.

Crucible Development

One major problem in casting silicon in silica crucibles is their bonding at high temperatures which results in cracking during the cool-down cycle. In clear crucibles invariably there appears to be attachment of the crucible to the ingot with a visible brown deposit, presumably SiO, sandwiched in between. A sample from run 89-C was examined with SEM. Figure 1 shows a micrograph of the boundary with cracking in the crucible as well as in the ingot. Microcracking is observed all along the interface. A visual examination showed that a dark brown band was present almost parallel to these cracks. The EDAX indicated that the silicon counts in the three regions (Figure 2) to be as shown in Table I. A comparison of these data with the silicon counts calculated for Si=100%, SiO=64%, and SiO_2=46% indicates that the brown deposit is probably SiO.

TABLE I. EDAX COUNTS IN THREE AREAS OF FIGURE 2

POSITION	MATERIAL	Si COUNTS/ UNIT TIME	NORMALIZED Si COUNTS/ UNIT TIME
Upper left corner	Silica, SiO_2	457	37
Middle	Brown interface	869	71
Lower right corner	Silicon, Si	1225	100

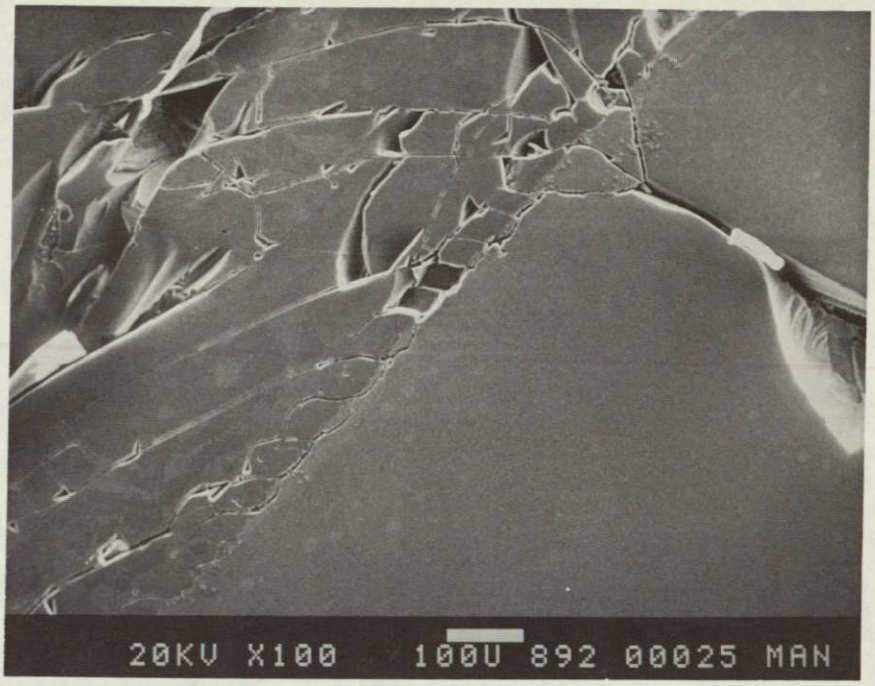

Figure 1. SEM examination of silica/silicon interface

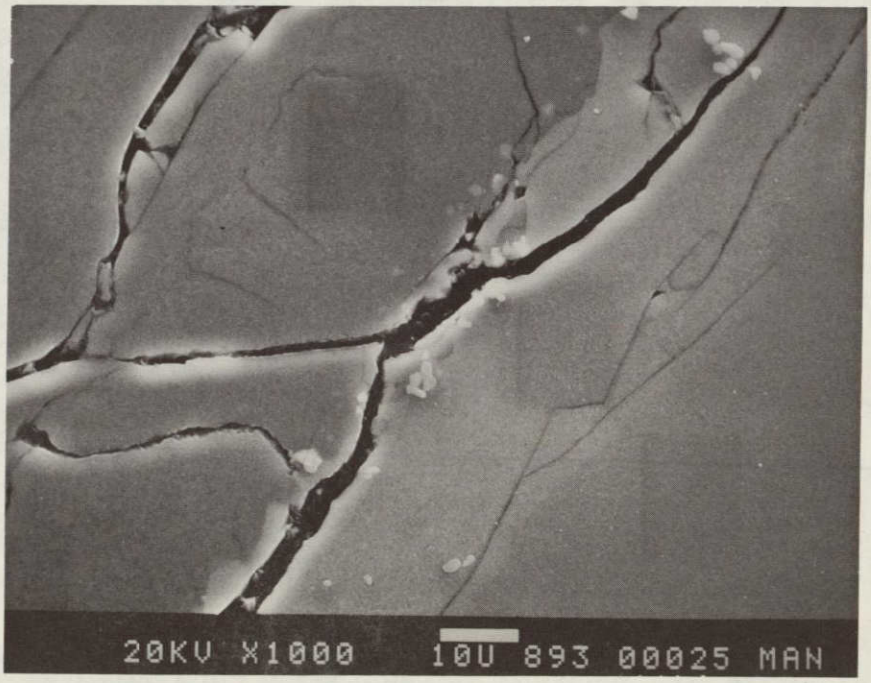

Figure 2. A higher magnification of Figure 1 showing areas where EDAX counts were taken

A sample of run 88-C was examined with SEM. During this run power failure resulted in rapid cooling of the melt. Very strong attachment of the silicon and silica was observed with no visual signs of the brown SiO layer. Figure 3 shows a firm crack-free type of bond for this sample. These results show that silica bonds to silicon. However, under the experimental conditions a SiO layer is formed at the interface. Since SiO is volatile at the melting point of silicon, it is not continuous; hence, bonding still results which causes cracking during the cool-down cycle.

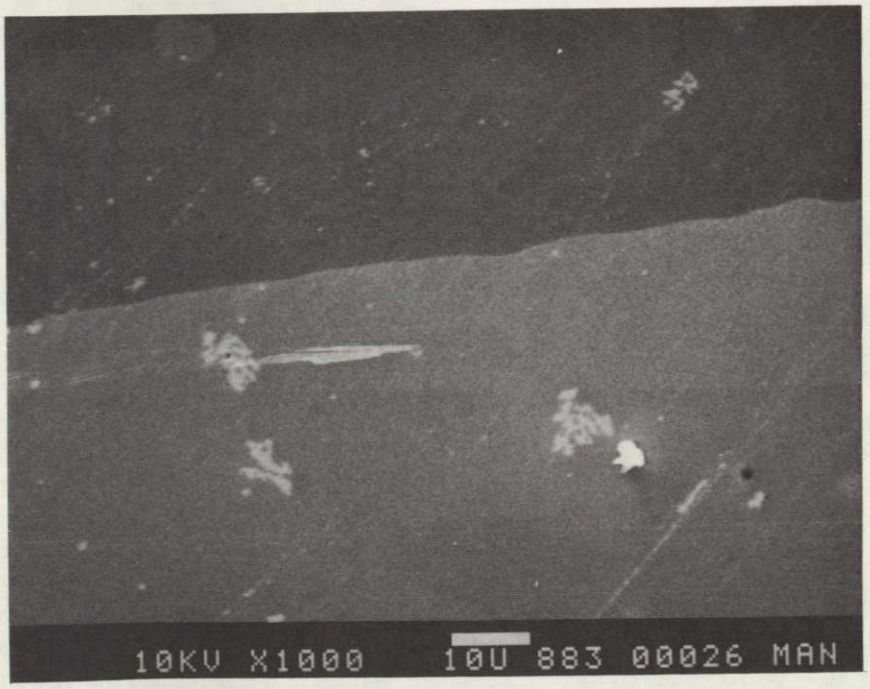

Figure 3. An area of the interface showing strong bonding of silica and silicon.

Different kinds of sintered crucibles have been used to cast silicon. It has been found that, unlike in the case of clear crucibles, the fused silica crucibles showed attachment only in some areas. Further, directional solidification was a more severe test for cracking--ingots that solidified crack-free without this condition were found to be cracked when a similar crucible was put on the heat exchanger. Phase identification and density measurements were carried out for these crucibles and the results are shown in Table II. The samples were taken from the top portion of the crucible which was not in contact with silicon after the experimental run. A study of Table II shows that even though different methods of processing, various particle sizes, with and without binder additions, were used to produce different starting densities, the final product after the run was very similar and too dense to fail during the cool-down cycle before cracking the ingot. In addition to the above-mentioned fused silica crucibles, candle quartz was also used which converted to distorted cristobalite and high quartz showed similar densification.

Detailed optical microscopic examination of the interface formed was carried out for three kinds of crucibles, viz., hot pressed, 8 μm slip cast, and 25 μm slip cast. These samples were examined at different magnifications and under normal light as well as various degrees of

TABLE II. PHASE IDENTIFICATION AND DENSITY OF VARIOUS FUSED SILICA CRUCIBLES

VITREOUS SILICA CRUCIBLE	PHASE PRESENT AFTER RUN	DENSITY	
		gms/cc	% THEORETICAL (BASED ON 2.32)
Slip cast, technical grade	Distorted Cristobalite		
Slip cast, high purity grade	Distorted Cristobalite	2.29	98.7
Slip cast, 200-mesh AS	Distorted Cristobalite	2.21	95.3
Slip cast, 200-mesh LS	Distorted Cristobalite	2.19	94.4
Hot pressed	Distorted Cristobalite	2.28	98.3
Pressure slip-cast, 8 μm	Distorted Cristobalite	2.26	97.4
Pressure slip-cast, 25 μm	Distorted Cristobalite	2.24	96.6
Coating, 65% 3 μm LS	Distorted Cristobalite	2.17	93.5
Coating, 68% 3 μm LS	Distorted Cristobalite	2.19	94.4

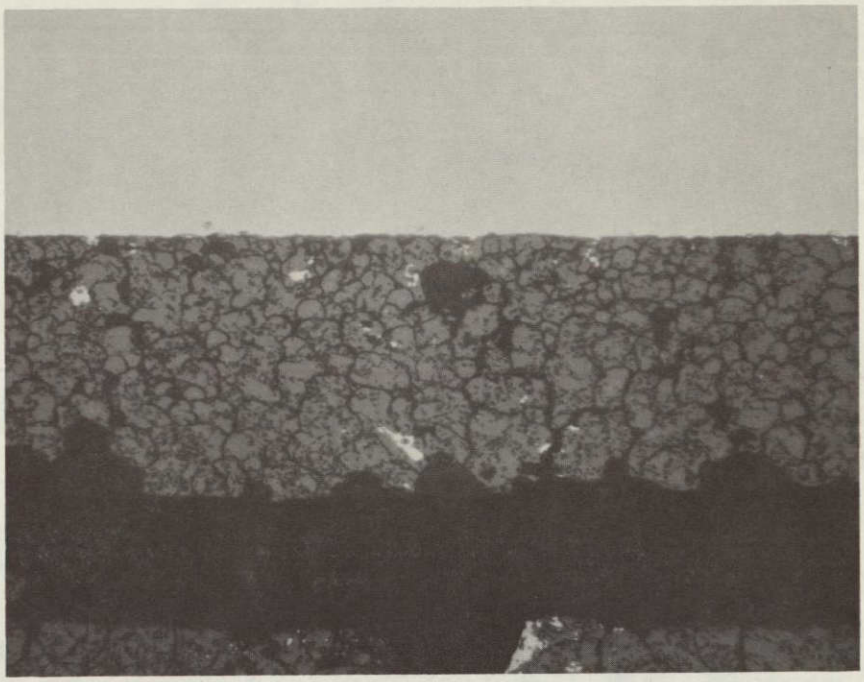

Figure 4. Optical micrograph (100X) under normal light for 8 μm pressure slip cast crucible

Figure 5. Optical micrograph (100X) under partial polarized light for 25 μm pressure slip cast crucible

Figure 6. Optical micrograph (100X) under polarized light for hot-pressed crucible

polarized light to show the different areas. All samples showed similar general features. Figures 4, 5, and 6 show the samples at 100X in different lighting conditions. The material well away from the interface had a typical silica structure with different grain sizes for the samples, as was expected. Near the interface some silicon carbide particles were seen, the concentration of which varied from place to place. The morphology of such a particle is shown in Figure 7. At the boundary a non-uniform thickness brown phase, presumably SiO, was observed. The least dense of these samples, 25 μm slip cast, showed SiO throughout the boundary (Figure 8) while the other two denser materials seemed to have less build up of this brown phase. Figure 9 shows an area where there is SiO next to an area where there is practically no brown deposit. This confirms the data reported above for x-ray diffraction and density measurements. It also explains the evidence of attachment only in certain areas of the sintered fused silica crucibles.

During last quarter[1] it was demonstrated that with the use of thin-walled clear fused silica crucibles the cracking during the cool-down cycle could be limited to the surface of the silicon ingot in contact with the crucible. The crack-free ingot obtained using this approach had a rough outside surface. In run 95-C (details in Table III) repeatability of this technique was attempted along with emphasis on

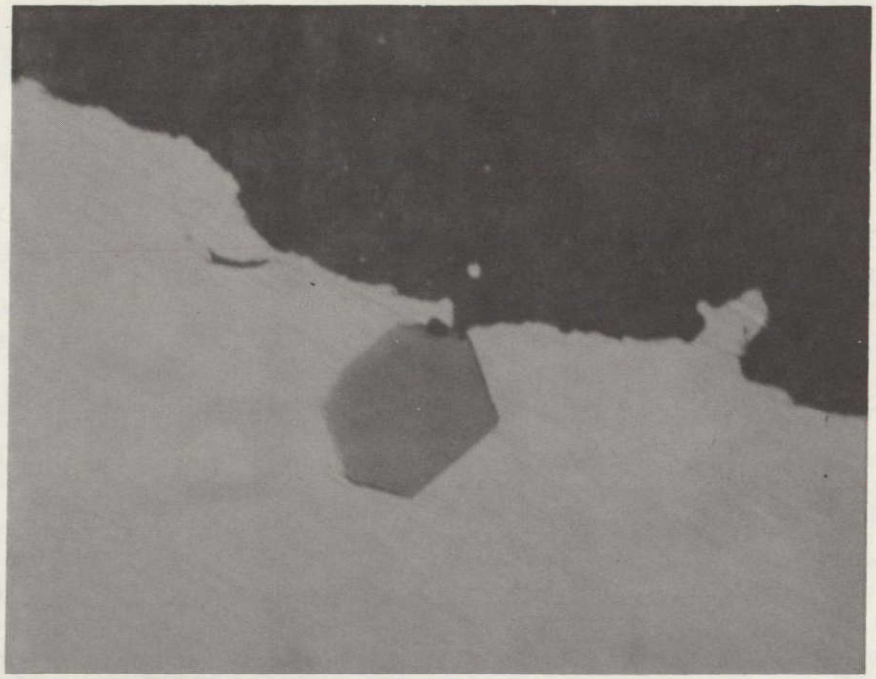

Figure 7. Optical micrograph (1000X) of a section of the 8 μm pressure cast crucible

Figure 8. Silica/silicon interface at 20X for 25 μm crucible. The grey area at boundary is SiO.

Figure 9. Non-uniform SiO (silky white area) in the hot-pressed crucible sample (500X)

TABLE III. TABULATION OF HEAT-EXCHANGER AND FURNACE TEMPERATURES

RUN	PURPOSE	SEEDING		GROWTH CYCLE			REMARKS
		FURN. TEMP. ABOVE M.P. °C	H.E. TEMP. BELOW M.P. °C	TEMP. DECREASE H.E. TEMP. °C/HR.	TEMP. DECREASE FURN. TEMP. °C	GROWTH TIME IN HOURS	
95-C	Achieve good growth using thin, clear crucible	7	59	179	11	9.8	Crack-free ingot cast. Good seed melt-back and growth above the seed and sides.
96-C	Prevent cracking using graded slip-cast high purity crucible	4	187	-	-	-	Power terminated during growth. Silicon penetrated through the crucible.
97-C	Prevent cracking using graded slip-cast technical grade crucible	3	120	165	2	4.0	Crack-free silicon cast.
98-C	Study effect of grading in slip-cast technical grade crucible	3	120	164	2	6.8	Silicon cracked into pieces. Indicates that heat treatment prevents cracking.
99-C	Prevent cracking using graded, spray-coated crucible.	3	120	170	0	3.3	Silicon cracked in areas where coating did not adhere to the crucible.
100-C	Prevent cracking using graded, opaque crucible	4	76	171	5	8.0	Crack-free boule cast (1.5 kg)

TABLE III. TABULATION OF HEAT-EXCHANGER AND FURNACE TEMPERATURES (Cont.)

RUN	PURPOSE	SEEDING		GROWTH CYCLE			REMARKS
		FURN. TEMP. ABOVE M.P. °C	H.E. TEMP. BELOW M.P. °C	TEMP. H.E. TEMP. °C/HR.	DECREASE FURN. TEMP. °C	GROWTH TIME IN HOURS	
101-C	Seeded growth using graded, opaque crucible	3	86	174	3	8.5	Crack-free boule cast (2.6 kg)
102-C	Prevent cracking using graded, coated crucible	5	90	147	5	5.2	Silicon cracked. Coating removed up to melt level.
103-C	Prevent cracking using translucent graded crucible	4	77	171	4	7.0	Crack-free ingot with no attachment of crucible.
104-C	Prevent cracking using translucent graded crucible	5	63	159	7	9.25	Ingot cracked because of attachment to areas of crucible with non-uniform graded structure.
105-C	Improve heat transfer using a graphite plug at bottom of crucible	-	-	-	-	-	Run terminated as crucible failed before reaching melt temperature.
106-C	Confirm experimentally if graphite retainer is source of SiC	-	-	-	-	-	Only Si around graphite piece showed SiC formation.

TABLE III. TABULATION OF HEAT-EXCHANGER AND FURNACE TEMPERATURES (cont.)

RUN	PURPOSE	SEEDING		GROWTH CYCLE			REMARKS
		FURN. TEMP. ABOVE M.P. °C	H.E. TEMP. BELOW M.P. °C	RATE OF DECREASE H.E. TEMP. °C/HR.	RATE OF DECREASE FURN. TEMP. °C	GROWTH TIME IN HOURS	
107-C	To form a compression fit between graphite plug and crucible	12	64	172	10	1.75	Crucible warped and silicon leaked out.
108-C	To form a compression fit between graphite plug and crucible	6	79	166	0	2.25	Crucible warped around plug. The seed bonded to the graphite.
109-C	Casting large Si ingot in opaque graded crucible (3.3 Kg)	8	89	138	7	12.0	Crack-free ingot cast
110-C	Improve heat transfer using graphite plug	11	96	106	2	6.0	No leakage around plug. Crack-free boule cast.
111-C	Improve heat transfer using graphite plug	-	-	-	-	-	Crucible failed when most material was molten. Run aborted. No leakage around plug.
112-C	To cast a crack-free single crystal boule	12	84	-	7	8.75	H.E. thermocouple malfunction. Helium flow at maximum from one-half hour into growth cycle. Crack-free boule cast.

TABLE III. TABULATION OF HEAT-EXCHANGER AND FURNACE TEMPERATURES (cont.)

RUN	PURPOSE	SEEDING		GROWTH CYCLE			REMARKS
		FURN. TEMP. ABOVE M.P. °C	H.E. TEMP. BELOW M.P. °C	RATE OF DECREASE H.E. TEMP. °C/HR.	RATE OF DECREASE FURN. TEMP. °C	GROWTH TIME IN HOURS	
113-C	Casting crackfree boule in opaque graded crucible (type II)	14	54	160	14	16	Crackfree boule cast. Seed melted out.
114-C	Casting single crystal crackfree boule	17	72	-	17	13.75	Crackfree boule cast. Seed melted out.
115-C	Testing of ultra-sonics to monitor liquid/solid interface	12	68	170	12	9.25	Most of silicon cast as single crystal but cracked on cooling due to bonding with crucible
116-C	Casting a 4 kg boule in opaque graded crucible (type II)	-	-	-	-	-	Run aborted due to loss of vacuum.

achieving good single crystal growth. A crack-free ingot was cast even though the crucible failed near the top towards the end of the solidification cycle. A polished and etched cross-section of this ingot is shown in Figure 10. It can be seen that most of the material solidified as single crystal.

Even though crack-free ingots can be cast in thin-wall clear crucibles there seems to be a problem of crucible failure before complete solidification. Further, the surface of the ingot is very rough which may involve grinding prior to slicing for solar cells. It was felt, therefore, that maintaining the integrity of the crucible during melt-down and solidification cycles is as important as its failure during cool-down cycle. Thus the crucible has to be strong enough to hold at high temperatures but weak enough to fail during the cool-down. In addition it should not bond to the silicon and cause surface cracking. A solution within the above limitations is a graded, sintered crucible. This crucible has full density on the inside surface to prevent penetration and grades to a low density on the O.D. for low compressive strength. In run 97-C a graded, slip-cast crucible was developed which produced a crack-free ingot (Figure 11). To confirm that the graded structure was essential, run 98-C was made with a same size crucible without the graded structure under similar conditions. This

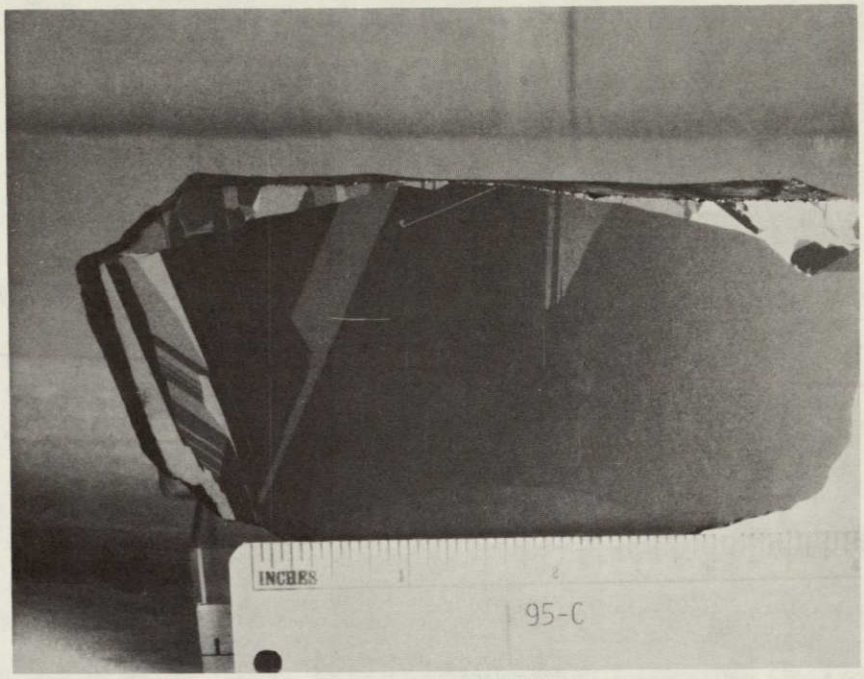

Figure 10. Polished and etched section of run 95-C.

Figure 11. Crack-free ingot cast in run 97-C.

ingot was cracked.

Having demonstrated that a graded crucible was essential to cast sound, acceptable ingots, larger melts were made in runs 100-C (1.5 kg) and 101-C (2.6 kg) using graded, opaque, silica crucibles. The ingots cast are shown in Figures 12 and 13 respectively. Both ingots are free of cracks and there is no surface roughness as obtained with clear crucibles. It has also been demonstrated with these experiments that shaped silicon crystals can be grown by the Heat Exchanger Method.

Since the graded approach seems to yield good results for slip-cast as well as opaque crucibles, it was felt that it should be tried with crucible coatings as well. In run 99-C two types of coatings--8 μm and 3 μm particle size--were treated to form a graded structure. These were smaller experimental melts. It was found that the coating did not adhere uniformly and cracks developed in the silicon wherever it was in direct contact with the clear crucible. In run 102-C a thicker graded spray coating was applied and a larger charge was used. The interior was sand blasted before coating to get better adherence. During this experiment there seemed to be a lot of reaction between the silicon and the coating which was indicated by a poorer vacuum. Higher furnace temperatures were essential to maintain usual melt temperatures because of loss of heat due to this reaction. It was found that most of the coating was

Figure 12. As-cast ingot in run 100-C (1.5 kg)

Figure 13. Crack-free ingot in run 101-C (2.6 kg)

eroded up to the melt level and the ingot cracked.

In run 109-C (Table III) an opaque graded crucible was used to cast a 3.3 Kg crack-free silicon boule (Figure 14). In this experiment extra insulation was added on the sides up to about three-fourths of the melt level. A polished and etched cross-section of this boule (Figure 15) shows that melt-back of the seed was achieved only on the sides and growth was promoted along the crucible wall. A clear demarcation at the top can be seen which coincides with the differences in insulation.

So far an opaque graded crucible has been found to be satisfactory. In runs 103-C and 114-C a translucent graded crucible has been used and a crack-free ingot cast (Figure 16). In run 113-C another form of a graded opaque crucible has been used to cast a crack-free ingot.

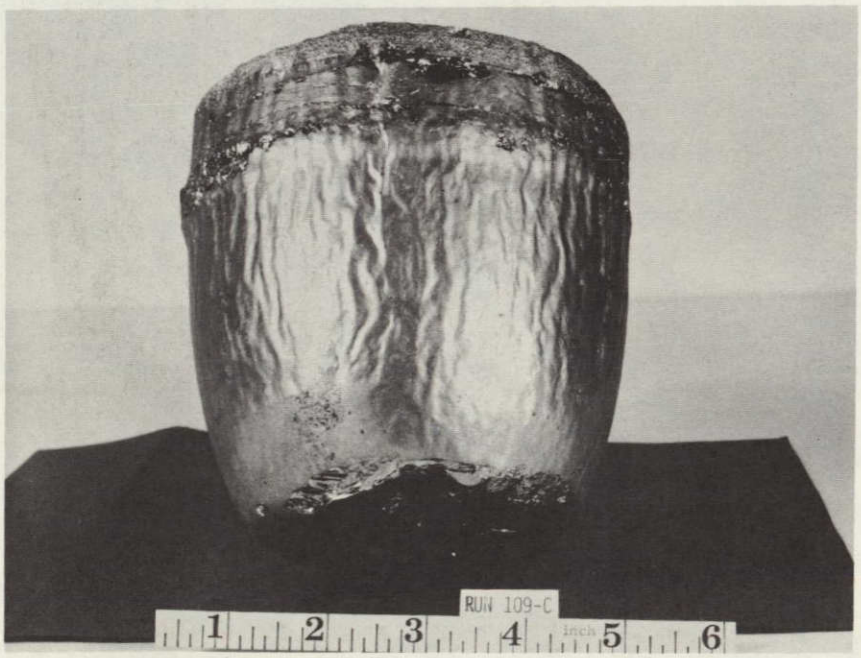

Figure 14. A crack-free 3.3 Kg silicon boule cast in run 109-C

Figure 15. Polished and Etched Section of Boule 109-C Showing Melt-back and Growth on the Sides of the Seed. The effect of insulation can be seen in the top section.

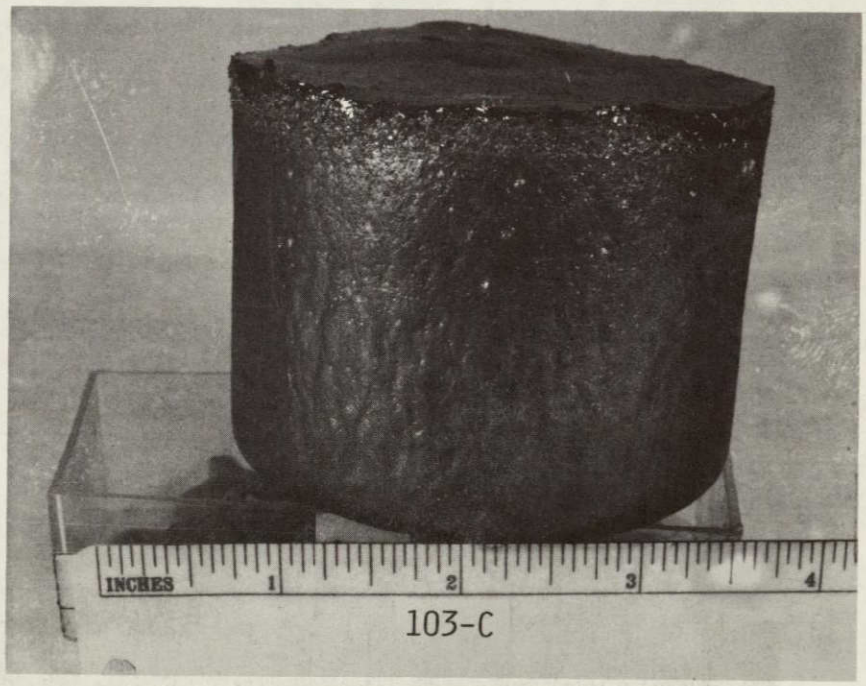

Figure 16. A Crack-free Silicon Boule Cast in Run 103-C Using A Graded, Translucent Silica Crucible

Material from 95-C was used to make 2 cm x 2 cm solar cells. The measured resistivity of the material of 0.6 ohm-cm. Data from four of the cells is shown in Figure 17 and Table IV. The cell properties show good consistency. The V_{oc} and fill factor values are fairly good when compared to material of high quality silicon in this resistivity range. The I_{sc} values are low especially in the long wavelength response, probably from unwanted impurities from the crucible and furnace during crystal casting. The conversion efficiency of these cells was about 8% (AMO) corresponding to more than 9% (AM1).

TABLE IV

I-V PARAMETERS (AMO)

(DVM Readings)

INGOT	CELL #	Voc (mV)	Isc (mA)	Tu (mA)	Xe (mA)	I_{400} (mA)	I_{450} (mA)	CFF*	L (mils)	W (mils)
95C	1	570	103.2	50.5	46.9	96.7	91.6	.70	781	782
	7	565	105.5	56.4	47.3	96.0	88.9	.69	782	782
	8	572	104.6	56.0	46.9	99.1	94.3	.70	781	782
	9	569	104.3	55.6	46.9	100.2	96.2	.72	782	782
	Control	584	130.2	77.2	53.2	128.9	126.2	.74	782	781

*Not at max. power (at 450 mv)

Source of Formation of Silicon Carbide - Theoretical

1. Introduction

Silicon crystals are grown in 0.1 torr vacuum by the Heat Exchanger Method (HEM). There is experimental evidence to show that silicon monoxide (SiO) and silicon carbide (SiC) are by-products of the process. Oxygen, silicon and carbon are used in this method in the form of silicon melt stock, silica crucibles and graphite furnace parts and retainers. In an effort to understand the reactions taking place in vacuum at high temperatures and to find ways to eliminate undesirable products of reactions, detailed thermodynamic calculations are initiated. Summary of thermochemical data used for analysis is shown in Table V.

2. Sources of Thermochemical Data Employed in the Analysis

Table V summarizes the thermochemical data required to carry out the calculations of oxygen solubility. These data are taken from several standard sources, supplemented by the ManLabs--NPL DATABANK and are believed to represent the best current description available.

TABLE V

SUMMARY OF THERMOCHEMICAL DATA*

(Temperature Range 1300°K to 1800°K)

Compound	Standard Free Energy of Formation (cal/mol)
SiC (solid)	-18,200 + 3.0T, T = °K
CO (gas)	-28,300 - 20.0T
CO_2 (gas)	-94,700
SiO_2 (solid)	-218,300 + 43.0T
SiO (gas)	-27,100 - 18.0T

The free energy difference between 1/2 O_2 (gas) at one atmosphere and O disolved in liquid silicon is:

$$-86000 + 28.0T + RT \ln N \text{ cal/mole of } \underline{O} \text{ where}$$

T = °K, R = 1.9873 cal/mol°K and N is the atomic fraction of oxygen. Thus if the number of oxygen atoms per cubic cm is N_A then $N = N_A \div (6.03 \times 10^{23} \times 2.33 \text{ gms/cm}^3 \div 28.09 \text{ gms/mole}) = N_A \div 5 \times 10^{22}$. The solubility of oxygen in silicon (in equilibrium) with SiO_2 is equal to 4×10^{-6}, 8×10^{-6} and 18×10^{-6} atom fractions at 1273°K, 1373°K and 1523°K respectively. These concentrations correspond to 2×10^{17}, 4×10^{17} and 9×10^{17} oxygen atoms/cm³ at the above noted temperatures.

*References: JANAF THERMOCHEMICAL TABLES.
ManLabs -NPL Data Bank.
O. Kubaschewski and T. G. Chart, J. Chem. Thermo (1974), 6 467 and "Constitution of Binary Alloys-First Supplement" R. P. Elliot McGraw Hill, New York, 1965.

3. Consideration of the Reaction between Liquid Silicon and Silica Crucible

The first problem which must be considered is the possible interaction between liquid silicon and the silica crucible at temperatures in the range 1685°K to 1735°K and at pressures in the 0.01 to 1.0 torr range. Figure 1 shows the results obtained by considering the reaction

$$Si\ (cond.) + SiO_2\ (cond.) \rightarrow 2\ SiO\ (gas) \qquad (1)$$

The free energy change for Equation (1), ΔG can be calculated from the data given in Table I as

$$\Delta G = \Delta G^\circ + 2RT\ \ell n\ p(SiO) \qquad (2)$$

where T = °K and p (SiO) is the pressure of gaseous SiO in atmospheres. Making the conversion from atmospheres to torr (760 torr is equal to one atmosphere) yields the following result:

$$\ell og\ p\ (SiO)\ torr = 11.47 - 17900T^{-1} \qquad (3)$$

Figure 1 shows the result of Equation (3) in dividing the temperature - pressure regime into a region where the reaction shown in Equation (1) proceeds to the right (forming SiO and consuming the crucible.) and a second range where the crucible containing the liquid silicon is stable. The present working range appears to lie in a range where SiO (gas) is stable thus leading to consumption of the crucible.

4. Consideration of the Reaction between Liquid Silicon and Silica Crucible

If the reaction between liquid silicon and the crucible is carried out in an environment where oxygen is released as in Equation (4), then the temperature - pressure regimes shown in Figure 18 will be altered. In particular, if

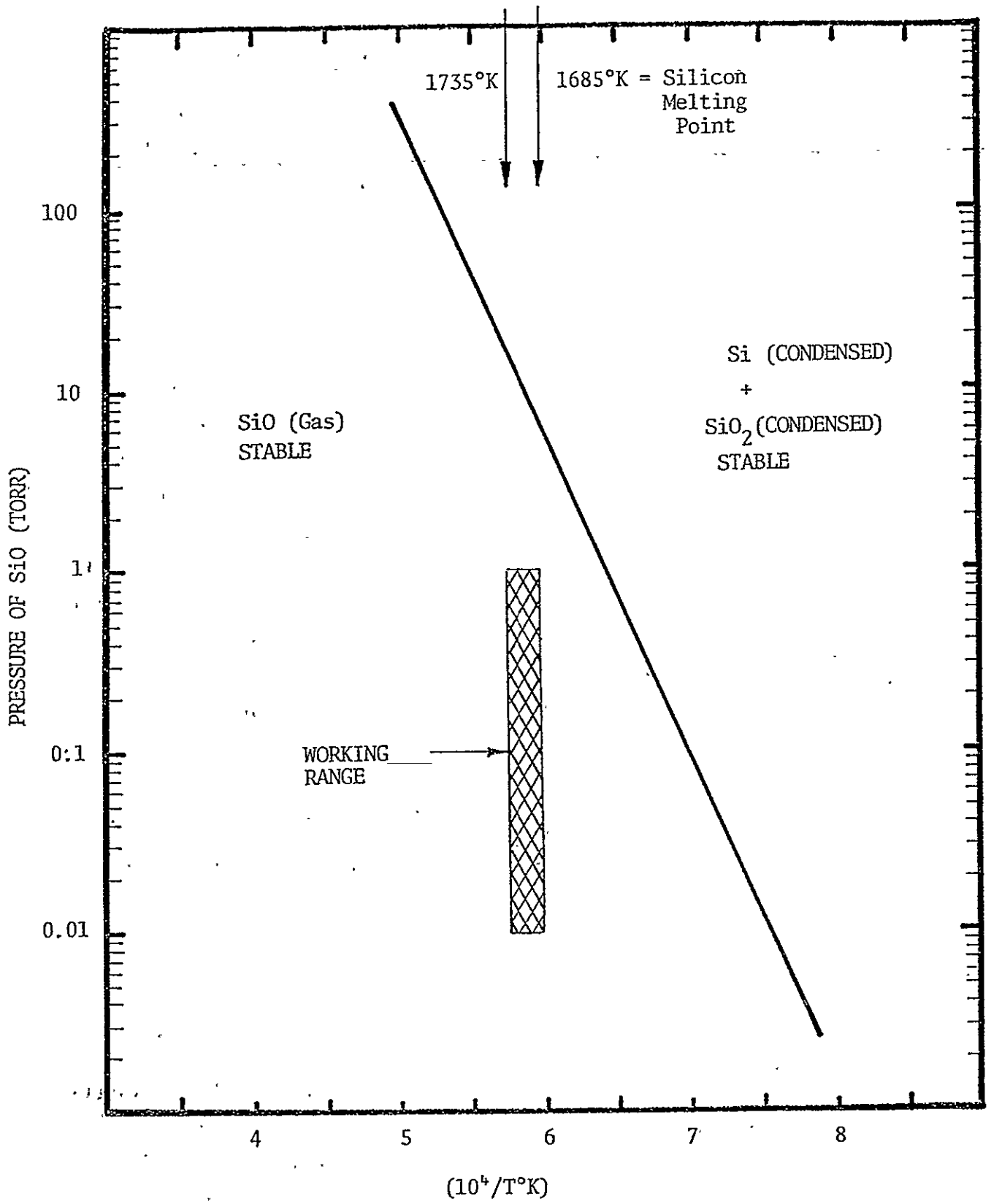

Figure 18. Equilibrium Vapor Pressure of Gaseous SiO as a Function of Temperature for the Reaction Si (CONDENSED) + SiO_2 (CONDENSED) $\rightarrow$ 2SiO (gas).

$$Si\ (cond.) + 3SiO_2\ (cond.) \rightarrow O_2 + 4SiO\ (gas) \qquad (4)$$

then the pressure of SiO will be equal to four times the pressure of oxygen and the total pressure P_T in torr will be given by Equation (5) on the basis of data shown in Table I.

$$\ell og\ P\ (total)\ (torr) = 11.78 - 23850T^{-1} \qquad (5)$$

Equation (5) leads to the results shown in Figure 2 which discloses that the phase boundary between the stable condensed phases and stable gaseous ranges has now shifted from above the working range to below the working range. Thus, on the basis of Figure 19 crucible decomposition would not occur in contrast to Figure 18 which suggests that crucible decomposition will occur on the basis of reaction 1.

Unfortunately, the environment in which the melting of silicon in silica crucibles is being carried out at present (i.e., in graphite furnaces) favors Equation (1) over Equation (4). This can readily be seen by considering the general equilibrium between CO and CO_2 under the conditions characterized by the proposed working range.

5. Examination of the CO/CO_2 Equilibrium in the Working Range

The data contained in Table 1 can be employed to examine the reaction

$$C\ (cond.) + CO_2\ (gas) \rightarrow 2\ CO\ (gas) \qquad (7)$$

Since

$$\Delta G = \Delta G^\circ + RT\ell n\ P^2_{CO}/P_{CO_2} \qquad (8)$$

and $\Delta G^\circ = 38100 - 40T$ calories, the reaction proceeds strongly to the right at 1700°K and pressures near 1 torr (i.e., 10^{-3} atmospheres). Thus CO will be the dominant species. This conclusion would be even stronger if graphite were to react

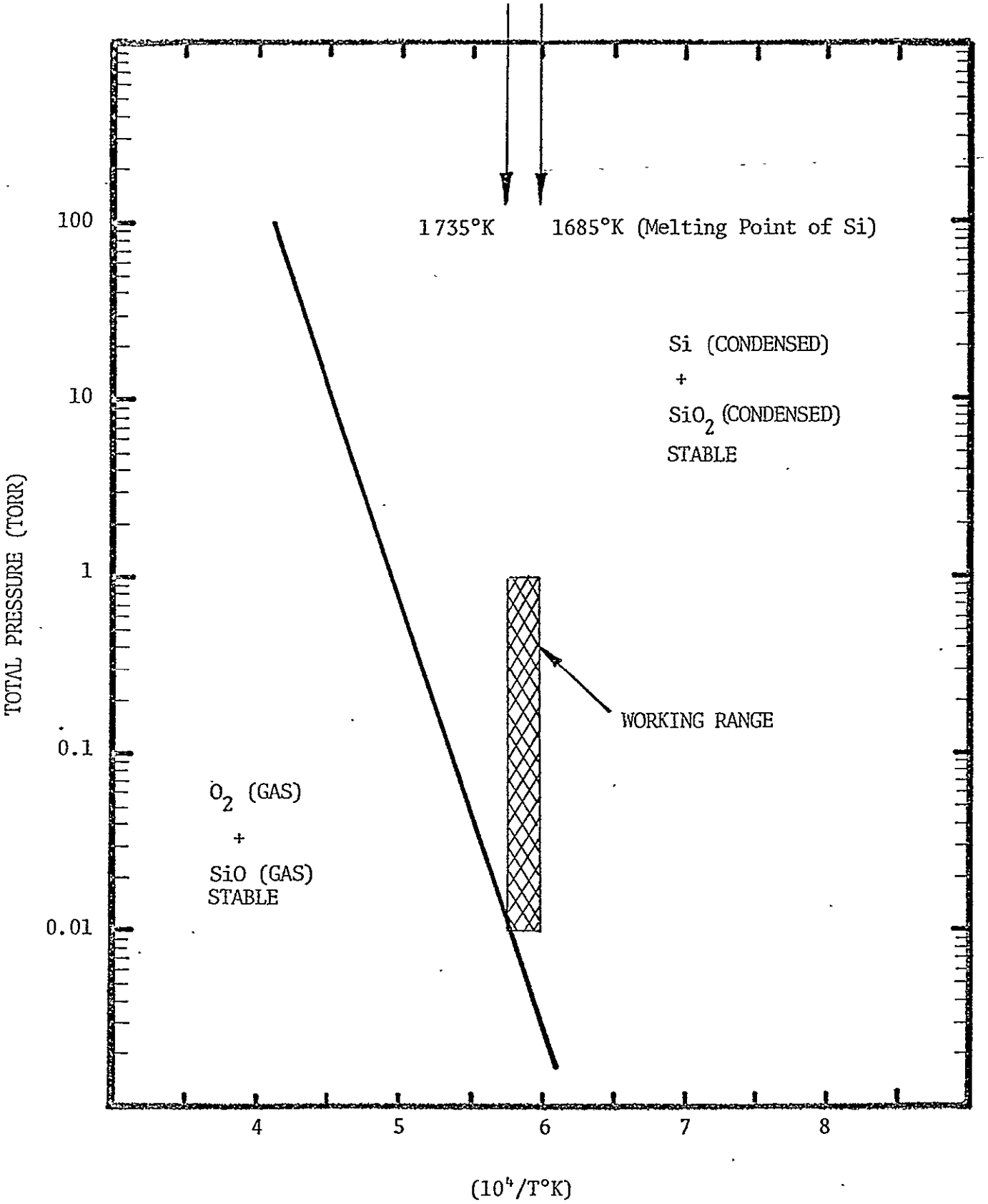

Figure 19. TOTAL EQUILIBRIUM VAPOR PRESSURE OF SiO AND O_2 FOR THE REACTION $Si(CONDENSED) + 3\ SiO_2\ (CONDENSED) \rightarrow O_2 + 4SiO\ (GAS)$.

with oxygen in place of CO_2 in Equation (7).

The conclusion reached on the basis of Equations (1) through (8) and Figures 18 and 19 is that a reaction between the silica crucible and molten silicon is likely to occur under the present working conditions on the basis of Figure 18 which represents a better description of the environment than Figure 19. This reaction might be suppressed by operating at a slightly higher pressure (i.e., 10 torr) and restricting the conditions to the range where the condensed gases in Figure 18 are more stable than the gaseous phases. The remaining question is what are the resulting levels of oxygen concentration in the silicon to be expected under these conditions. This question is addressed in Sections 6 and 7 below.

6. Evaluation of the Reaction between Oxygen Dissolved in Silicon with Silicon to Form Gaseous SiO

Table V contains a characterization of the reaction between oxygen dissolved in liquid silicon and silicon to form SiO (gas) at one atmosphere. At lower pressures, this reaction can be characterized by means of Equation (9), where $T = °K$, $P(SiO)$ (torr) is the pressure and N is the atomic fraction of oxygen in silicon. Table V shows that if $N = 10^{-5}$ then the number of oxygen atoms per cm^3 (of silicon) is 5×10^{17}.

$$\log \frac{P\ (SiO)}{N}\ (\text{torr}) = 12.93 - 12870T^{-1}. \qquad (9)$$

The results of Equation (9) are displayed in Figure 3 showing the phase boundaries for the formation of SiO (gas) as a function of pressure, temperature and the concentration of oxygen in silicon. Figure 20 also displays the crucible decomposition boundary derived in Figure 18. Reference to Figure 20 suggests that rather low concentrations of oxygen could be attained at the low pressure end of the working range. However, this re-

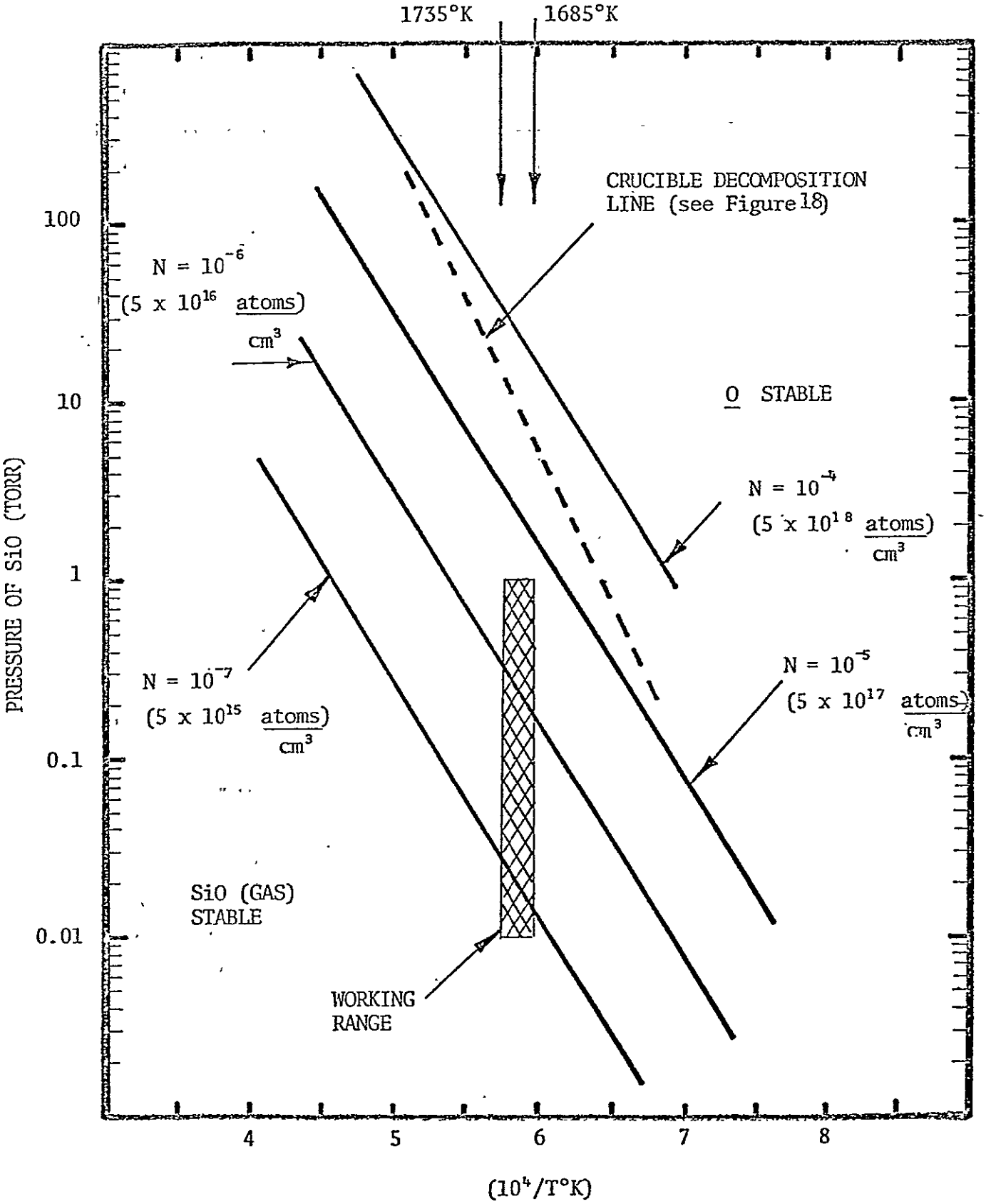

Figure 20. EQUILIBRIUM BOUNDARY FOR THE REACTION O (DISSOLVED OXYGEN) + Si (CONDENSED)→SiO (GAS) AS A FUNCTION OF OXYGEN CONCENTRATION (IN ATOMIC FRACTION AND ATOMS/cm^3).

sult will be conditioned by the crucible decomposition line. Thus at pressures near 10 torr and temperatures near 1700°K oxygen concentrations of 3×10^{18} atoms/cm^3 could be attained. Further lowering of the pressure would lead to lower oxygen concentrations until the crucible decomposition line is intersected. Under these conditions, the crucible would start to decompose providing further oxygen and prevent additional lowering of the oxygen concentration in solution. Additional examination of the oxygen level can be effected by considering the simultaneous role of carbon in this process. This analysis is presented in Section 7.

7. Consideration of the Simultaneous Reaction of Carbon and Oxygen in Liquid Silicon

Since the analysis of Section 5 established that CO will be the dominant vapor species in the oxidation of carbon it is of interest to consider the reaction

$$\underline{C} + \underline{O} \rightarrow CO \text{ (gas)} \qquad (10)$$

where $\underline{C}$ and $\underline{O}$ refer to carbon and oxygen dissolved in silicon. In order to evaluate the free energy change for the reaction in Equation 10 between carbon as graphite at one atmosphere and $\underline{C}$ (dissolved in silicon). This difference has been assessed as $-12700 + 9.5T + RT \ln N$ where N is the atom fraction of carbon in solution in silicon. Utilization of the data in Table V along with the fact that the equilibrium in Equation (10) requires equal number of carbon and oxygen in solution (for equilibration with CO) leads to the following result

$$\log p\,(CO)\ (\text{torr})\ N^{-2} = 15.45 - 15390T^{-1} \qquad (11)$$

where N is the atomic faction of oxygen or carbon. At

$T = 1710^{\circ}$ K

$$P\ (CO)\ \text{torr} = 2.8 \times 10^{6}\ N^{2} \qquad (12)$$

If $P = 0.028$ torr then $N = 10^{-4}$ or 5×10^{18} atoms/cm^3.

Note that this pressure lies below the crucible decomposition line in Figure 18.

8. Detailed Calculation of the Rate of Evaporation of Silicon Monoxide

The previous consideration of reactions between liquid silicon and silica yielded the following equations for the equilibrium vapor pressure of silicon monoxide arising from the reaction:

$$Si\ (cond.) + SiO_2\ (cond.) \longrightarrow 2\ SiO\ (gas) \qquad (1)$$

$$\log p\ (SiO)\ \text{torr} = 11.47 - 17900T^{-1}$$
$$\log p\ (SiO)\ \text{atm.} = 8.58 - 17900T^{-1} \qquad (3)$$

At 1712°K (i.e. 25°C above the melting point of silicon) Equation (3) yields an equilibrium vapor pressure of 1.31×10^{-2} atm or about 10 torr. In order to calculate the rate of Langmuir vaporization of silicon monoxide into a vacuum one can apply Equation (13) to compute the rate W in units of gms/cm^2 sec.

$$W\ (\text{gms/cm}^2\ \text{sec}) = 44.4\ p\ (\text{atm})\ M^{\frac{1}{2}}(SiO)\ T^{-\frac{1}{2}} \qquad (13)$$

where M (SiO), the molecular weight of silicon monoxide in grams is equal to 44, and T is the absolute temperature in Kelvins. Equation (13) yields an equilibrium rate of vaporization of 0.092 gms/cm^2 sec. under these conditions.

9. Comparison of the Calculated Rate with the Rate Observed During a Crystal Growth Experiment

In an experiment conducted at Crystal Systems, a 2500 gm weight of silicon was melted in a cylindrical clear silica crucible with a six-inch (15.24 cm) diameter and a flat bottom. The melt was kept at heat for about 24 hours at a pressure of about 0.5 torr and 1712°K. After the exposure, measurement of the crucible wall disclosed a uniform corrosion of about 0.04 cm.

Allowing for the thermal expansion of silicon to the melting point and a volume contraction of 1.4 cm^3/g. at. on melting the volume of the silicon at the melting point is approximately 938 cm^3. This volume suggests that the liquid cylinder in the silica crucible was 5.12 cm high (and 15.24 cm in diameter). The surface area of contact between the silicon melt and the silica crucible is 427 cm^2 composed of 182 cm^2 along the bottom and 245 cm^2 along the vertical walls.

The 0.04 cm wall recession translates into a total volume recession of 0.04 x 427 or 17 cm^3 of silica. Since the density of silica (SiO_2) is 2.65 gms/cm^3 the mass recession is equal to 45 gms. The reaction stoichiometry of Equation (1) demands that 88 gms of SiO be liberated for every 60 gms of SiO_2 consumed. Thus, the consumption of 45 gms of silica would lead to evaluation of 66 gms of SiO.

If one treats the entire surface area of the melt (182 cm^2) as the area through which SiO vaporizes then the vaporization

rate is 66 gms/182 cm^2 x 86400 seconds or 4.2×10^{-6} gms/cm^2 sec. This estimate depends on the nucleation of SiO bubbles at the silicon/silica wall and rapid migration to the melt surface. The observed evaporation rate is thus 0.042×10^{-4} gms/cm^2 sec. which is more than 20,000 times slower than the calculated equilibrium evaporation rate.

10. Consideration of Reactions between Graphite and Silica Crucible

Following reactions between graphite and silica crucible were studied.

$$3C + SiO_2 \longrightarrow SiC + 2CO \quad (14)$$

$$4C + 2SiO_2 \longrightarrow SiC + 3CO + SiO \quad (15)$$

$$C + SiO_2 \longrightarrow CO + SiO \quad (16)$$

$$C + 2SiO_2 \longrightarrow 2SiO + CO_2 \quad (17)$$

$$2C + SiO_2 \longrightarrow SiC + CO_2 \quad (18)$$

$$3C + 3SiO_2 \longrightarrow SiC + 2CO_2 + 2SiO \quad (19)$$

All the reactions have positive free energies at atmospheric pressure, as shown in Figure 21, with those reactions that produce CO_2 being the most positive.

Two reactions given by equations (14) and (16) gave the least positive free energies at atmospheric pressure. These were studied as a function of pressure and temperature:

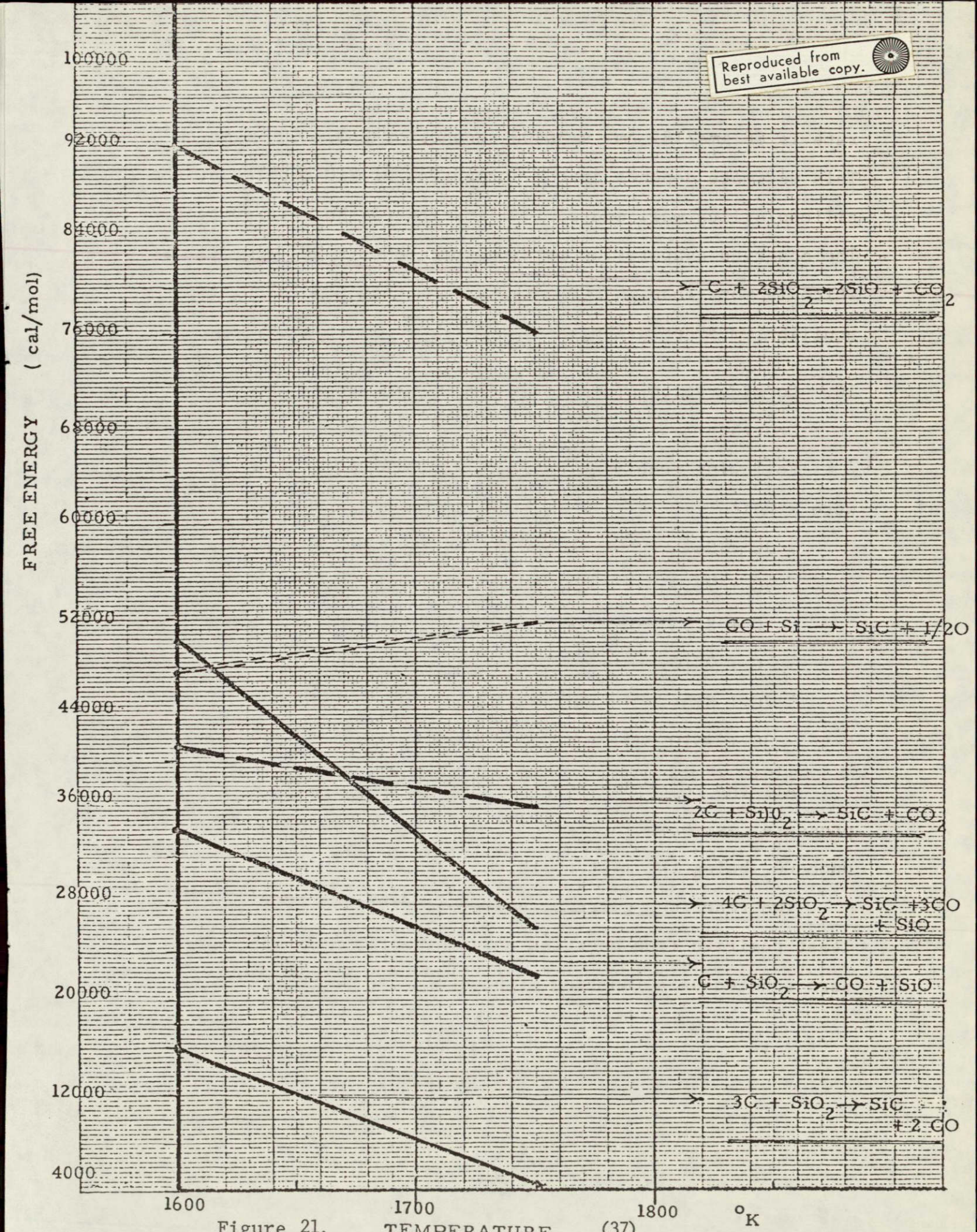
Reproduced from best available copy.
FREE ENERGY (cal/mol)
100000
92000
84000
76000
68000
60000
52000
44000
36000
28000
20000
12000
4000
1600
1700
1800
°K
TEMPERATURE
C + 2SiO2 → 2SiO + CO2
CO + Si → SiC + 1/2O
2C + SiO2 → SiC + CO2
4C + 2SiO2 → SiC + 3CO + SiO
C + SiO2 → CO + SiO
3C + SiO2 → SiC + 2 CO

Figure 21.

(i) $3C + SiO_2 \longrightarrow SiC + 2CO$ (14)

$\Delta G = \Delta G^o + RT\ln p_{CO}^2$

$\Delta G^o = 143500 - 80T$ (Using data in Table V)

Hence $\Delta G = 143500 - 80T + (4.575)(2)\log p_{CO}$ (atm)

$\Delta G = 0$ so that

$\log p_{CO}$ (atm) $= 8.74 - 1.57 \times 10^4/T$ (20)

Figure 22 shows the regions of stability of this reaction as a function of pressure and temperature.

(ii) $C + SiO_2 \longrightarrow SiO + CO$ (16)

$\Delta G = \Delta G^o + RT \ln (p_{SiO})(p_{CO})$

$\Delta G^o = 162900 - 81T$ (using data in Table V)

$\frac{1}{2}p = p_{SiO} = p_{CO}$

$\Delta G = \Delta G^o + RT \ln (p/2)$

$\Delta G = 0$ so that

$\log p$ (atm) $= 9.15 - 1.78 \times 10^4/T$

$\log p$ (torr) $= 12.03 - 178 \times 10^4/T$ (21)

The range of stability of this reaction is also shown in Figure 22.

Reaction (14) shows that SiC is formed by the reaction of carbon and silica but it does not explain how SiC is found in silicon. A common feature of reactions (14) and (16) is that under experimental conditions CO is the common stable species.

All data obtained from these studies of interaction of graphite with the silica crucible indicates that the SiC is not

formed in silicon because of these reactions. However, there is experimental evidence to show that silicon carbide is formed during the casting of silicon by the Heat Exchanger Method (HEM). Other possibilities could be the interaction of the by-products of the feasible reactions with themselves, or silicon. These reactions are analyzed in the following section.

11. Consideration of Reaction between CO and C with SiO

(i) The following reaction was studied:

$$CO + 3\ SiO \longrightarrow SiC + 2\ SiO_2 \qquad (22)$$

$$\Delta G = \Delta G^o - RT \ln (p_{CO})\ (p_{SiO})^3$$

$$\Delta G^o = -\ 345{,}200 + 163T \text{ (using data in Table V)}$$

$$P_t = p_{CO} + p_{SiO};\ p_{CO} = (1/3)\ p_{SiO}$$

$$\log P_t \text{ (torr)} = 12.04 - 10.89 \times 10^4/T \qquad (23)$$

The regions of stability of this reaction are shown in Figure 23. It can be seen that under the operating experimental conditions this reaction does not proceed to the right.

(ii) $$3C + 2SiO \longrightarrow 2\ SiC + CO_2 \qquad (24)$$

Reaction has a negative free energy a 1 atm, - 9818 cal/mole at 1600 K to -3720 cal/mole at 1750 K.

(iii) $$2C + SiO \longrightarrow SiC + CO \qquad (25)$$

Reaction has a negative free energy at 1 atm -17977 cal/mole at 1600 K to -17783 cal/mole at 1750 K.

(iv) $$C + 2\ SiO \longrightarrow 2Si + CO_2$$

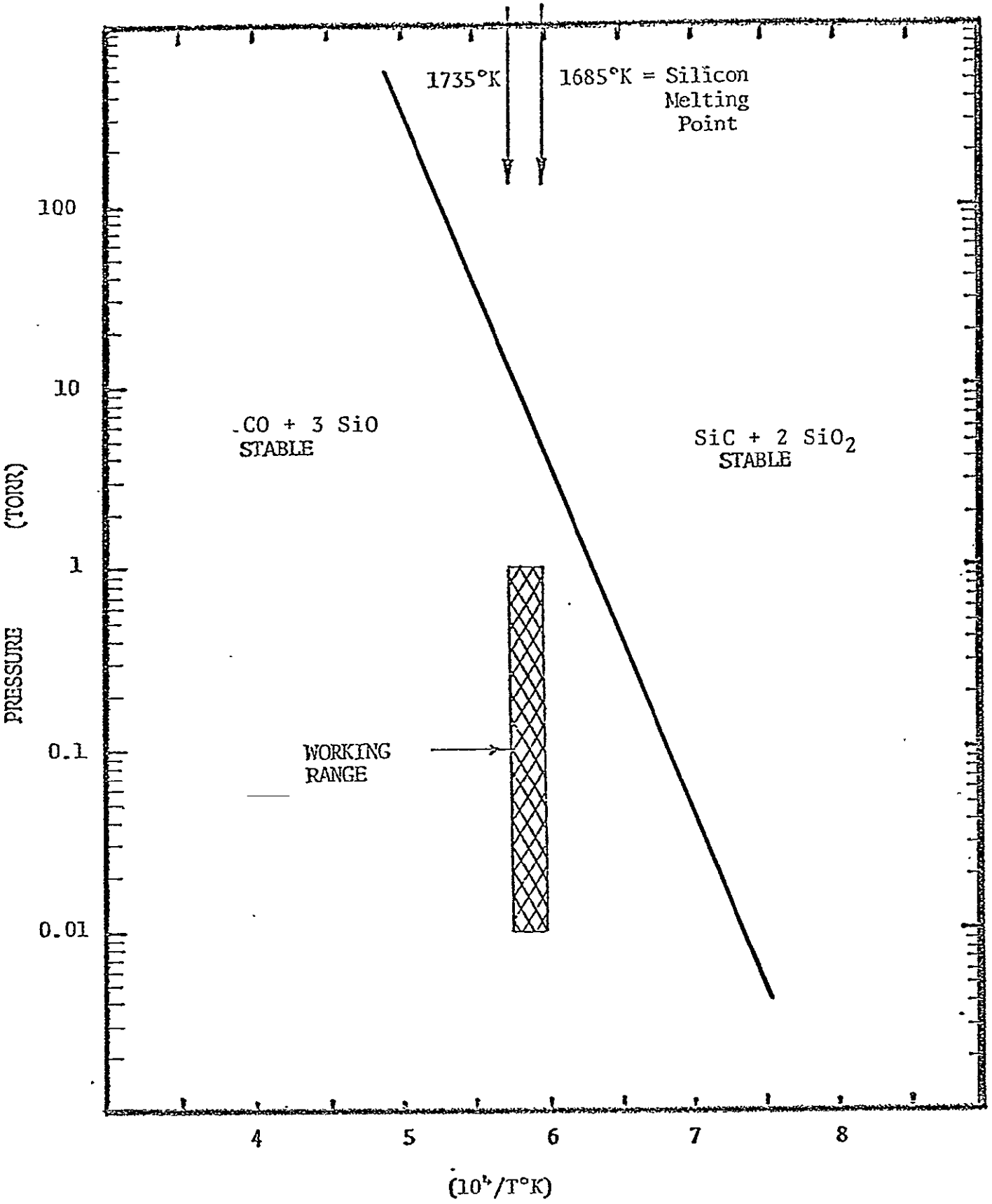

Figure 23. Equilibrium Total Pressure of CO and SiO as a Function of Temperature for the Reaction;

$$CO + 3\ SiO \rightarrow SiC + 2\ SiO_2$$

Reaction has a positive free energy at 1 atm

+16035 cal/mole at 1600 K to +20643 cal/mole at 1750 K

$$\text{(v)} \quad C + SiO \longrightarrow Si + CO \qquad (27)$$

Reaction has a negative free energy - 4870 cal/mole at 1600 K to -5602 cal/mole at 1750 K.

12. <u>Consideration of Reaction between CO or CO_2 with Silicon</u>

A number of reactions involving CO and CO_2 were studied.

$$\text{(i)} \quad CO + Si \longrightarrow SiC + \tfrac{1}{2} O_2 \qquad (28)$$

This reaction yields positive free energy at atmospheric pressure and is shown in Figure 21. It should be noted that the slope of energy vs. temperature for this reaction is positive as contrasted to the negative slopes for other reactions in Figure 21.

Calculations were made using pressure as a variable.

$$\Delta G = \Delta G^o + RT \ln p_{O_2}^{1/2} / p_{CO}$$

$$\Delta G^o = 10100 + 23T \text{ (using data in Table V)}$$

$$4.575 \log p_{O_2}^{1/2} / p_{CO} = -10100 - 23\ T$$

At T≃ 1700 K

$$p_{O_2}^{1/2} / p_{CO} = 4.68 \times 10^{-7}$$

$$p_{O_2} + p_{CO} = 1$$

let $x^2 = p_{O_2}$; $x - p_{O_2}^{1/2}$ and $p_{CO} = 1 - x^2$

$$\frac{x}{1 - x^2} = 4.68 \times 10^{-7}$$

$$p_{O_2}^{1/2} \sim 4.68 \times 10^{-7}$$

Even if the total pressure is reduced to 10^{-4} atm = 0.076 torr, this reaction will not proceed at 1700 K.

(ii) $CO_2 + Si \longrightarrow SiC + O_2$ (29)

Reaction has positive free energy of 81875 cal/mole at 1600° K to 82633 cal/mole at 1750 K.

(iii) $2CO + 3Si \longrightarrow 2\,SiC + SiO_2$ (30)

$\Delta G^{\circ} = -198100 + 89T$ (reaction proceeds to the right at 1 atm and 1700 K)

$\Delta G = \Delta G^{\circ} - RT \log p_{CO}$

$\log p_{CO}$ (torr) $= 12.6 - 2.17 \times 10^4/T$ (31)

The stability range of this reaction is shown in Figure 24. Under the working range the reactants are stable.

(iv) $CO + 2Si \longrightarrow SiC + SiO$ (32)

$\Delta G^{\circ} = -17000 + 5.0\,T$ (reaction proceeds to the right at 1700 K)

$\Delta G = -17000 + 5.0\,T + 4.575\,T \log p_{SiO}/p_{CO}$

P total $= p_t = p_{SiO} + p_{CO}$; $p_{CO} = (1-x)p_t$;

$p_{SiO} = x\,p_t$.

$\Delta G = -17000 + 5.0\,T + 4.575\,T \log (x/1-x)$

Reaction does not depend on pressure. The equilibrium fraction of SiO (i.e., x) is given by:

$$\exp\left\{\frac{17000-5T}{1.987\ T}\right\}\ \left\{1 + \exp\left\{\frac{17000\ -\ 5\ T}{1.987\ T}\right\}\right\}^{-1} = x$$

T K	$x = p_{SiO}/p_t$	%CO	%SiO
1650	0.935	6.5	93.5
1687	0.928	7.2	92.8
1700	0.925	7.5	92.5
1750	0.915	8.5	91.5

(v) $CO_2 + 2\ Si \longrightarrow SiC + SiO_2$ (33)

$\Delta G^o = -47100 + 46.0T$ (reaction <u>does</u> <u>not</u> go to the right. $\Delta G^o = 31100$ at 1700 K and 1 atm)

$\Delta G = \Delta G^o - 4.575\ T \log p_{CO_2}$

$\log\ p_{CO_2}$ (torr) $= 12.94 - 1.03\ (10^4/T)$ (34)

at $T = 1687$; $(10^4/T) = 5.92$

$\log p_{CO_2}$ (torr) $= 6.84$

$\log p_{CO_2}$ (atm) $= 4$; $p_{CO_2} = 10$ kilobars.

Reaction does not go to the right and there is practically no pressure effect.

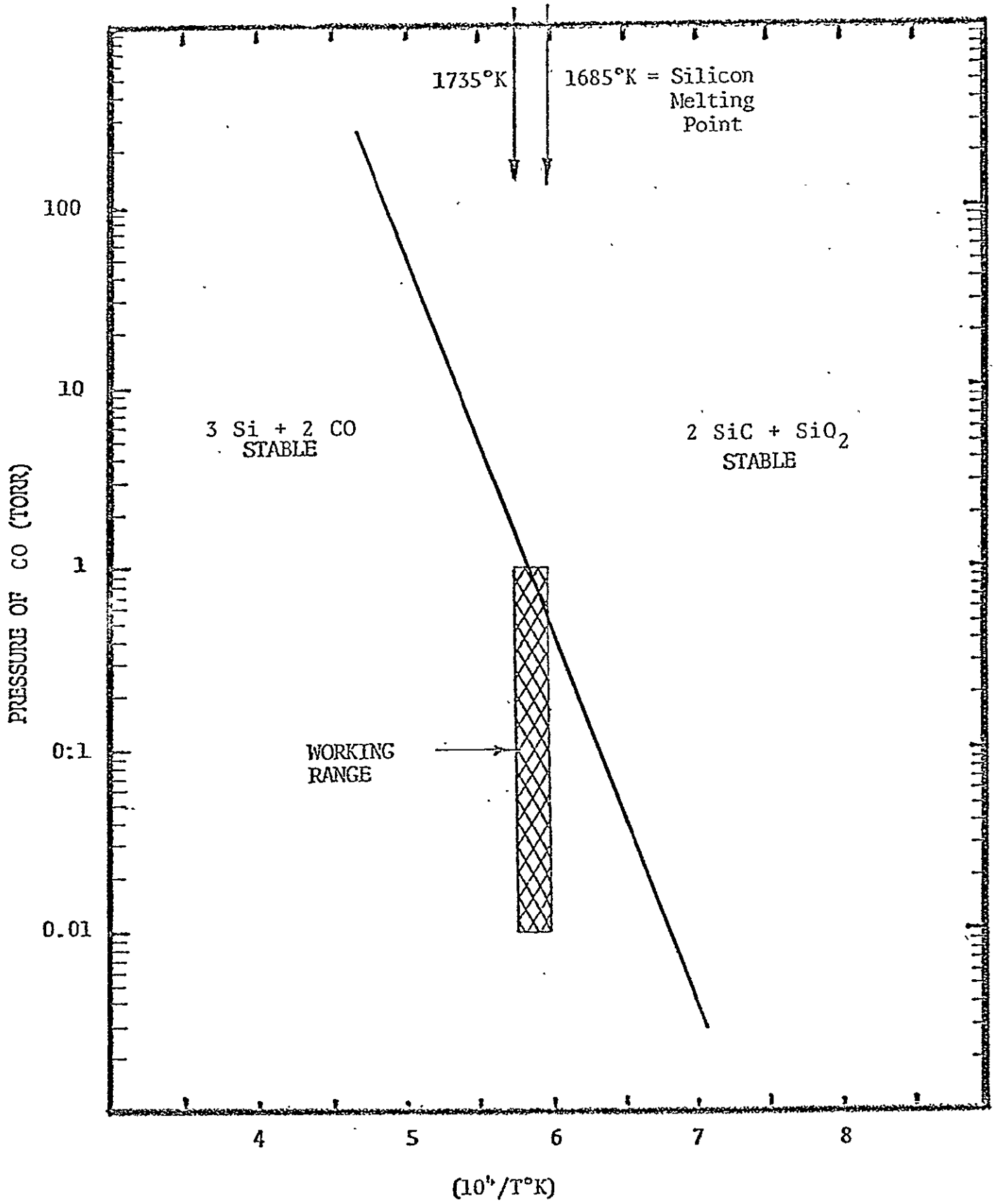

Figure 24. Equilibrium Pressure of CO as a Function of Temperature for the reaction;

$$2\ CO + 3\ Si \rightarrow 2\ SiC + SiO_2$$

(vi) $CO_2 + 3\ Si \rightarrow SiC + 2\ SiO$ (35)

$\Delta G° = +22300 - 33\ T$ (reaction goes to the right at one atm and 1700K)

$$\Delta G = \Delta G° + RT \ln p^2_{SiO}/p_{CO_2}$$

$$p_{SiO} = x\ p_t \quad ; \quad p_{CO_2} = (1-x)p_t.$$

$$\Delta G = 22300 - 46.2T + 4.575\ T \log p(torr) + 4.575\ T \log (x^2/(1-x))$$

at equilibrium $\Delta G = 0$

$$\ln (x^2/(1-x)) = \frac{-22300 + 46.2\ T - 4.575\ T \log p(torr)}{1.9873\ T}$$

at $T = 1700$ and $-2 \leq \log p \leq 3$

$x^2 \rightarrow 1$. Thus,

$$\ln (1-x) = \frac{22300 + 4.575\ T \log p_t(torr) - 46.2T}{1.9873\ T}$$

$$x = \text{fraction SiO} = 1 - \exp \left[\frac{22300 + 4.575\ T \log p_t(torr) - 46.2\ T}{1.9873\ T}\right]$$

at 1687K

$$= 1 - \exp \left[\frac{-55639 + 7718 \log p}{3353}\right]$$

p(torr)	x	%SiO
1	1.0	100%
10	-	-
100	-	-
1000	0.99994	99.994%

The reaction goes to the right and there is virtually no pressure effect.

Results

1. Silicon monoxide is formed by the silicon-silica reaction

$$Si + SiO_2 \longrightarrow 2\ SiO \qquad (1)$$

At the melting point of silicon SiO is volatile. This reaction could result in decomposition of the crucible; however, experimental evidence indicates that the reaction rate is about 20,000 times slower than the calculated equilibrium evaporation rate.

2. Silicon carbide is formed predominately by the reaction of carbon monoxide and silicon:

$$CO + 2\ Si \longrightarrow SiC + SiO \qquad (32)$$

The source of CO is from the graphite retainers used to support the crucible.

3. The CO is due to the reaction of the crucible and the graphite retainers; viz.,

$$3C + SiO_2 \longrightarrow SiC + 2\ CO \qquad (14)$$

$$C + SiO_2 \longrightarrow SiO + CO \qquad (16)$$

The furnace parts although made of graphite have been coated with silicon carbide and do not contribute to the formation of silicon carbide in the melt.

Source of Formation of Silicon Carbide - Experimental

In the above analysis it was shown that the most likely source of SiC formation is from reaction (32). The CO is evolved from graphite retainers. The furnace parts, although made of graphite, have been coated with silicon carbide and do not contribute to the formation of silicon carbide in the melt. In run 106-C (Table III) a graphite piece was sandwiched between two pieces of single crystal silicon with polycrystalline silicon around them. The furnace was heated to close to the melting point of silicon and cooled. It was found that a silicon carbide layer was formed in areas where the graphite was in contact with silicon crystals and also a light layer in the immediate vicinity. The pieces of polycrystalline silicon far removed from the graphite piece did not show any evidence of SiC. In this experiment the graphite piece was not in contact with silica; hence reactions (14) and (16) were suppressed. Consequently the polycrystalline silicon pieces were not coated with silicon carbide.

Efforts to Eliminate Silicon Carbide Impurities

In order to avoid reaction between graphite crucible retainers and silica crucibles used in the melting of large ingots of silicon, efforts are being made to reduce the tendency to form CO or CO_2 gas which can contaminate the silicon at high temperatures. One method of attacking this problem is to coat the retainer with silicon carbide in order to form a barrier between silica and graphite and limit the reaction. This study examined the possible ranges of temperature and pressure on which a reaction between the silica and silicon carbide coating can occur. Five following reactions were studied:

I $SiC + SiO_2 \rightarrow 2Si + CO_2$

Result: Reaction can go to the right depending on temperature and pressure. (See Figure 25.)

II $2SiC + SiO_2 \rightarrow 3Si + 2CO$

Result: Reaction can go to the right depending on temperature and pressure. (See Figure 26.)

III $SiC + SiO_2 \rightarrow SiO + CO + Si$

Result: Reaction can go to the right depending on temperature and pressure. (See Figure 27.)

IV $SiC + 2SiO_2 \rightarrow 3SiO + CO$

Result: Reaction can go to the right depending on temperature and pressure. (See Figure 28.)

V $SiC + SiO_2 \rightarrow C + 2SiO$

Result: Reaction can go to the right depending on temperature and pressure. (See Figure 29.)

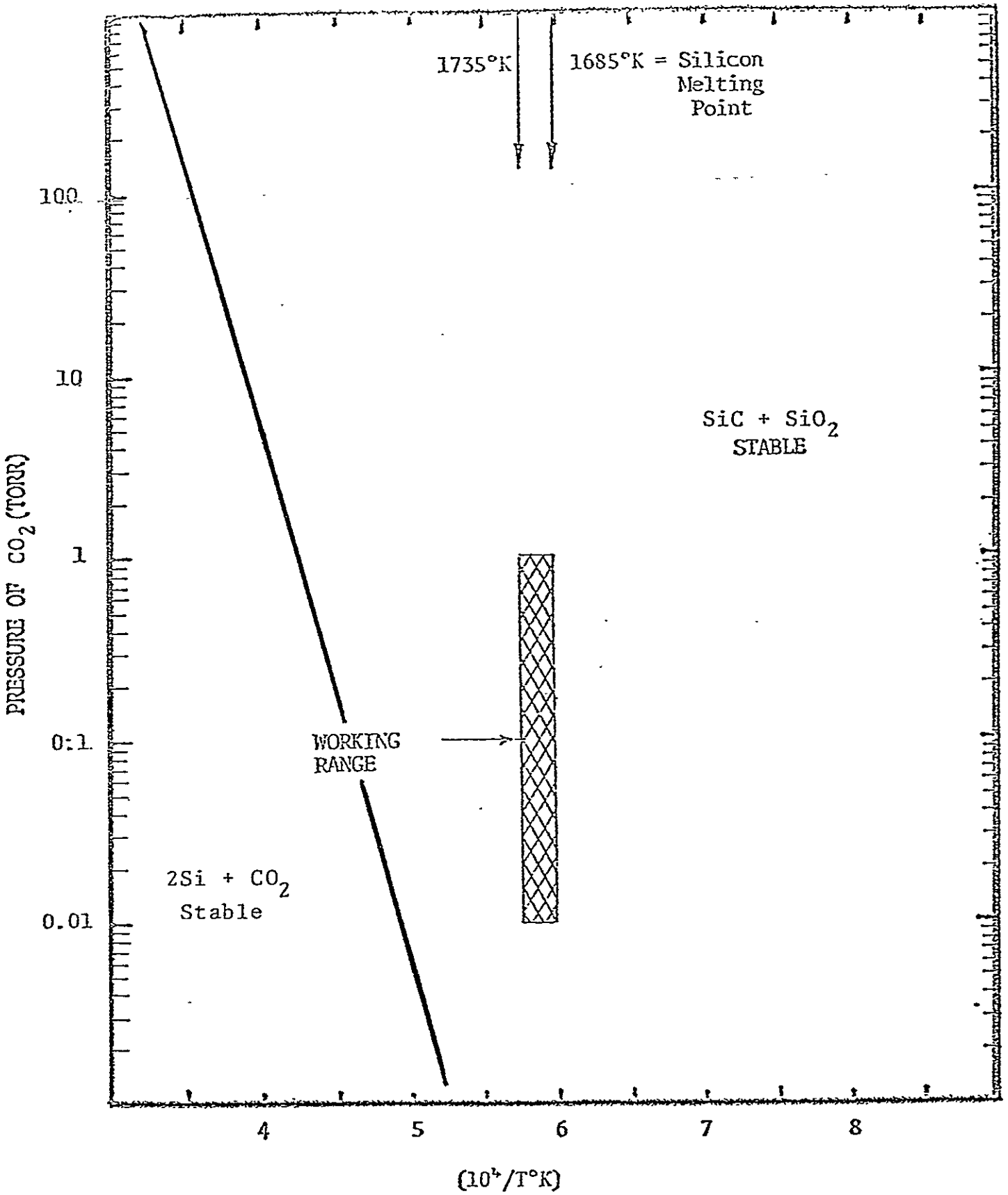

Figure 25. Equilibrium Pressure of CO_2 as a Function of Temperature for Reaction I;

$$SiC + SiO_2 \rightarrow 2Si + CO_2$$

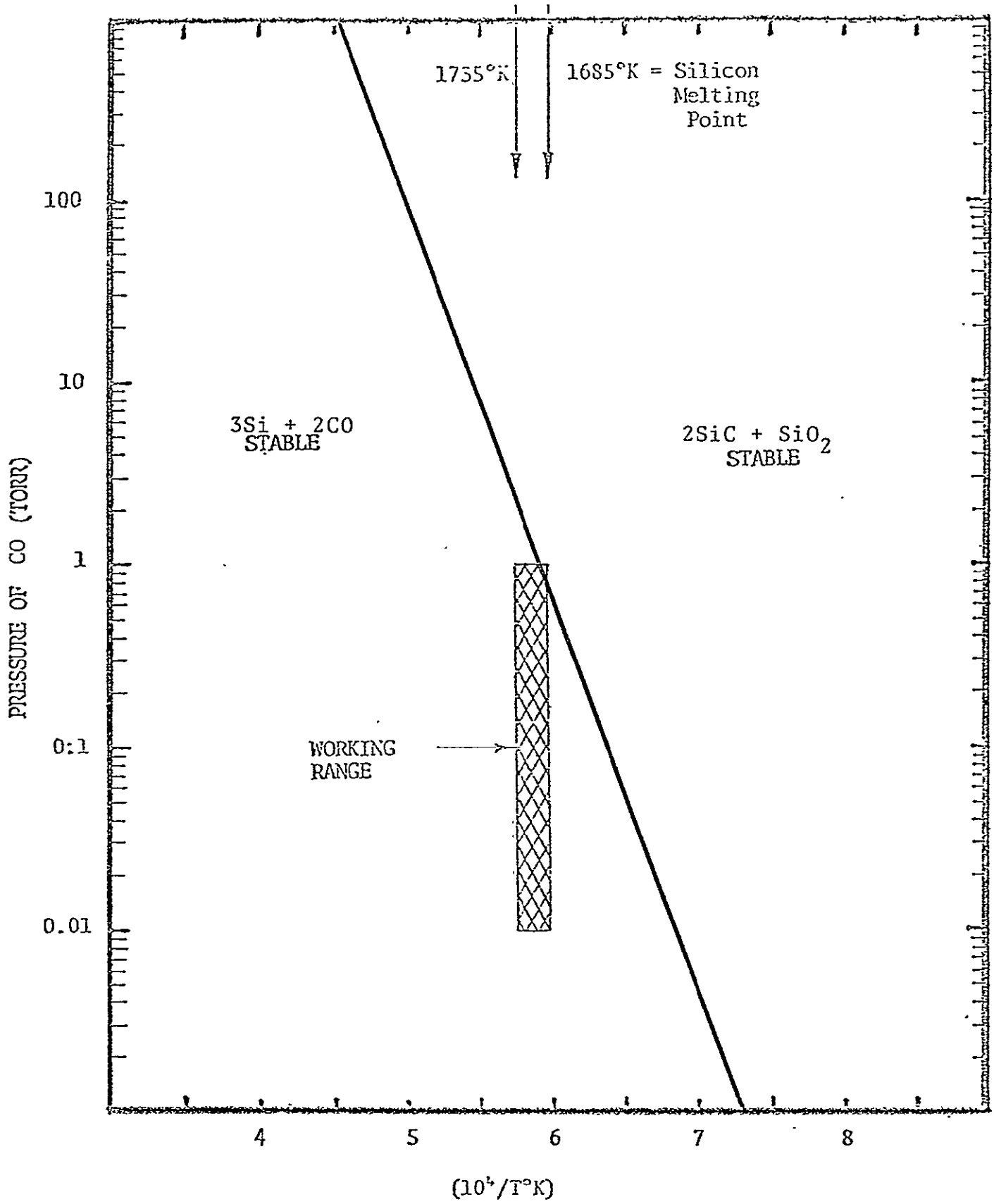

Figure 26. Equilibrium Pressure of CO as a Function of Temperature for Reaction II;

$$2SiC + SiO_2 \rightarrow 3Si + 2CO$$

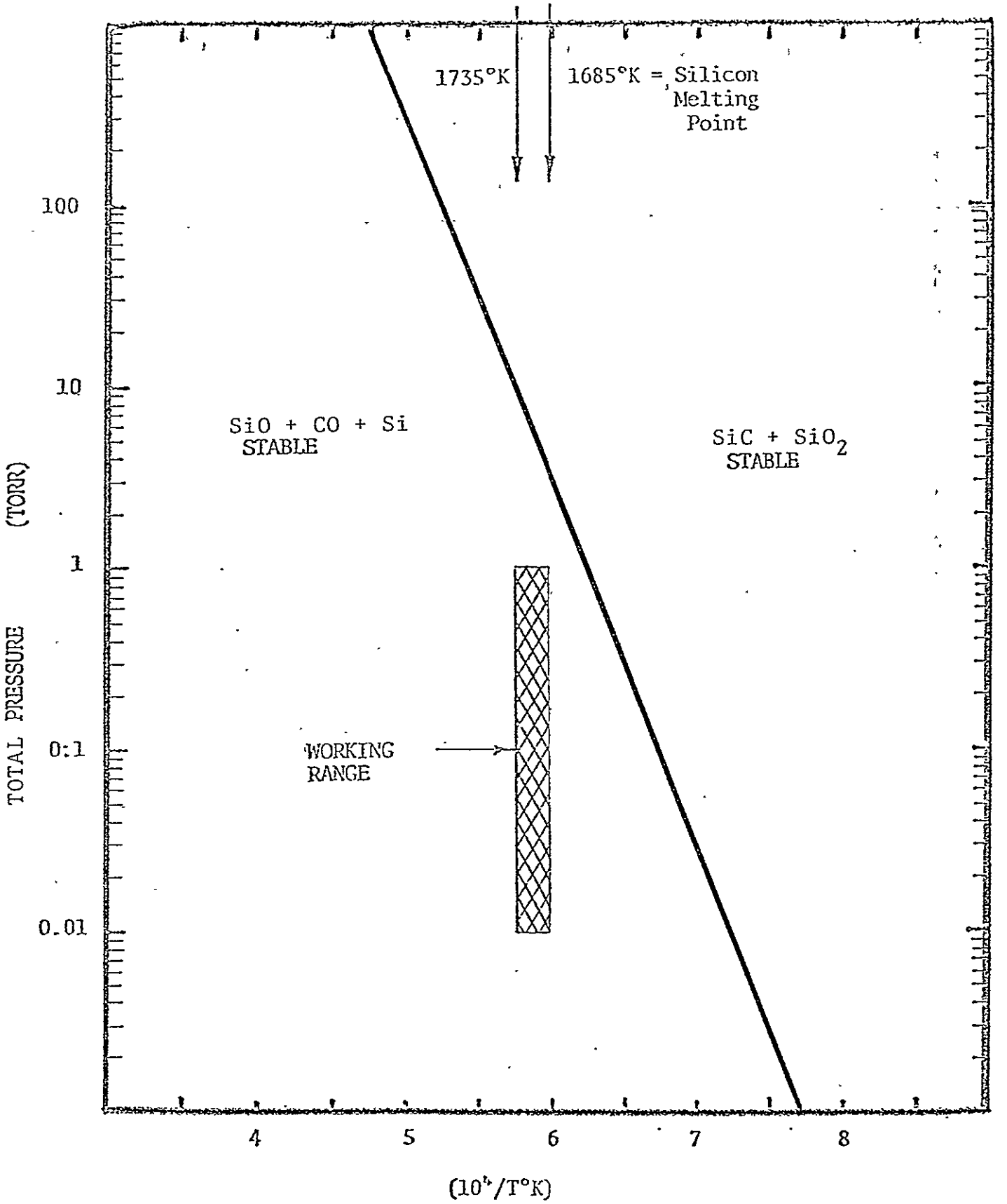

Figure 27. Total Pressure of SiO and CO as a Function of Temperature for Reaction III;

$$SiC + SiO_2 \rightarrow SiO + CO + Si$$

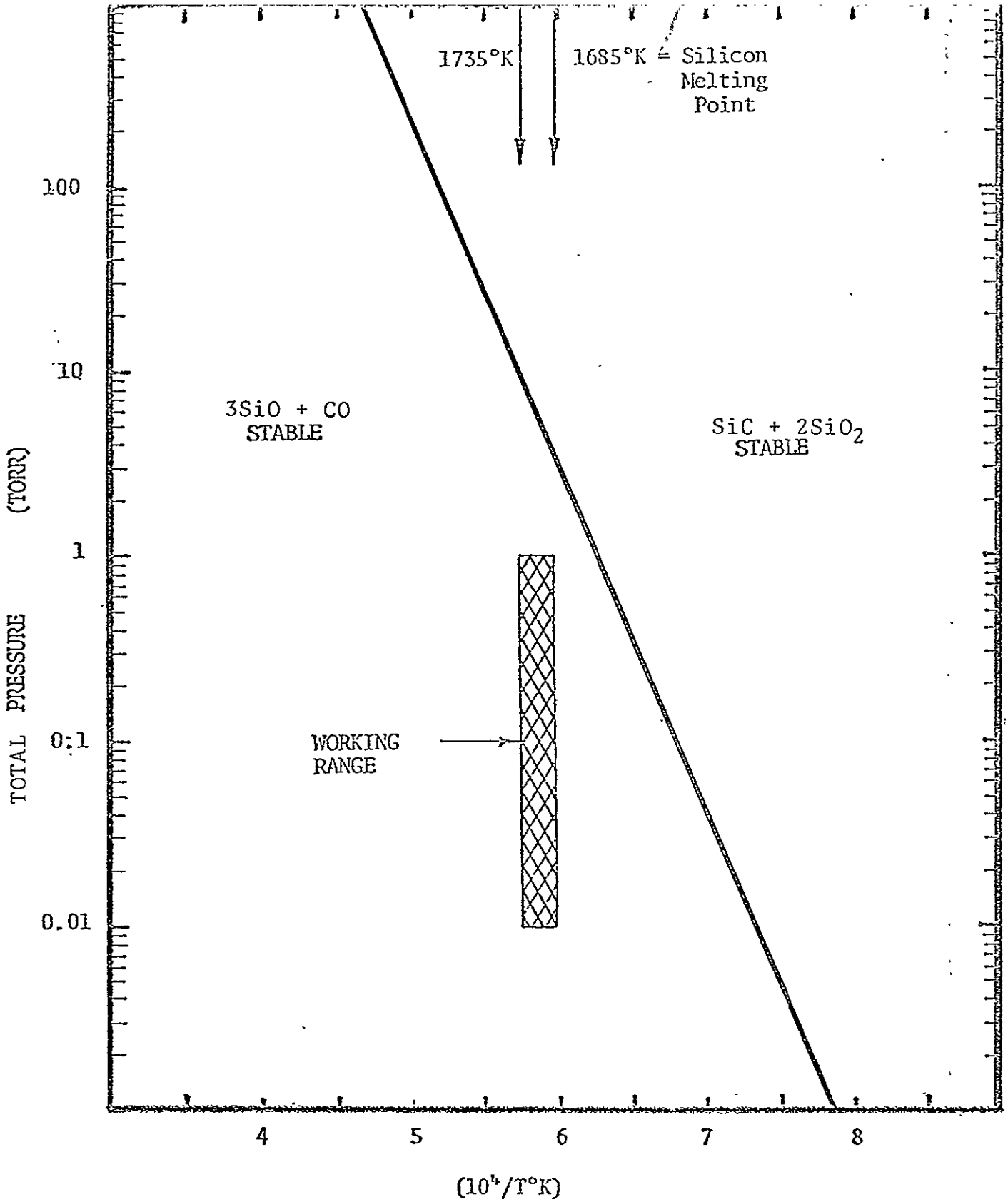

Figure 28. Total Pressure of SiO and CO as a Function of Temperature for Reaction IV;

$$SiC + 2SiO_2 \rightarrow 3SiO + CO$$

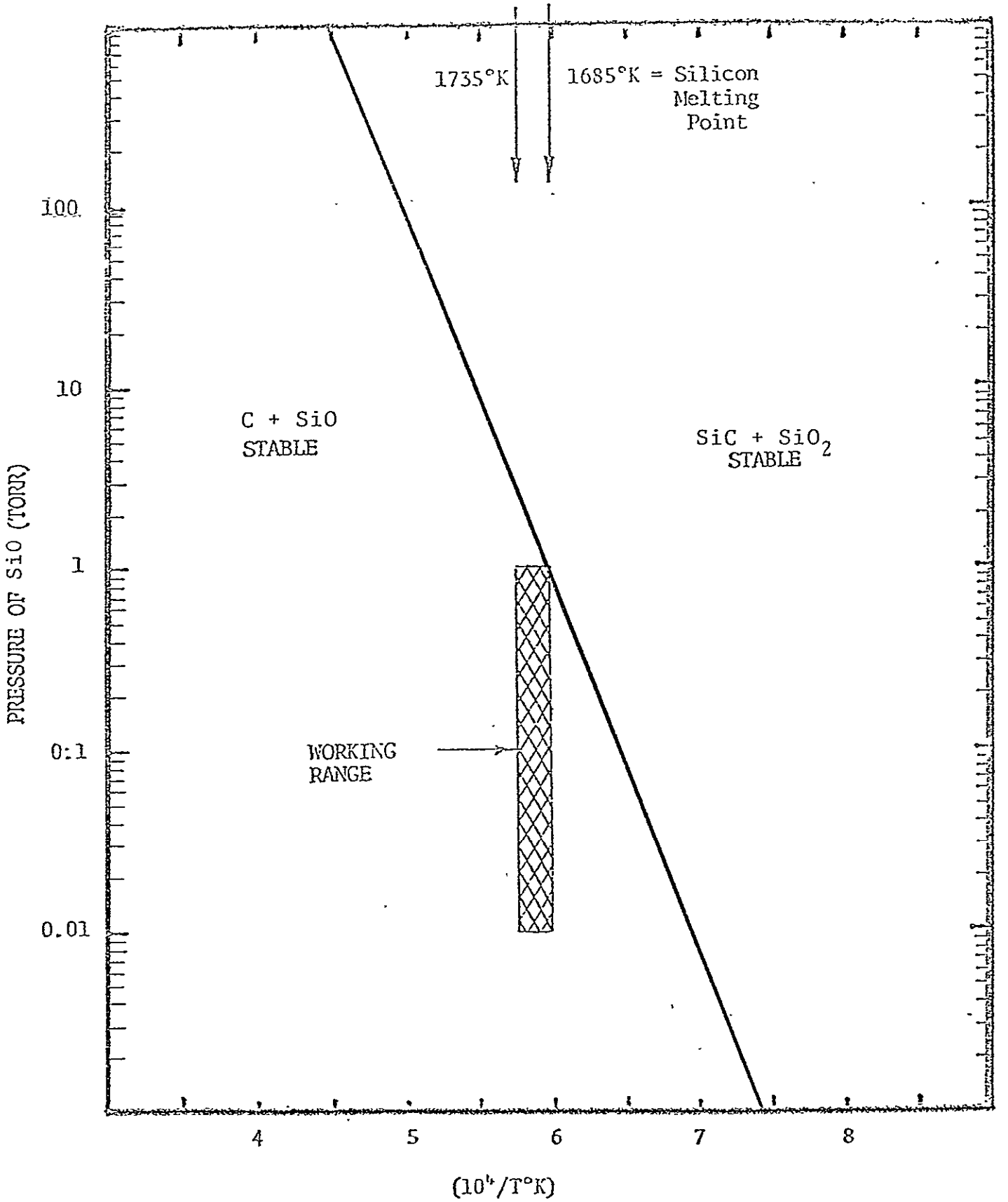

Figure 29. Equilibrium Pressure of SiO as a Function of Temperature for Reaction V;

$$SiC + SiO_2 \rightarrow C + 2SiO$$

REACTION I

$$SiC + SiO_2 \rightarrow 2Si + CO_2$$

$\Delta G° = 141600 - 47.0T = 61700$ (calories) at 1 atm., 1700K.

(reaction does not proceed to the right at one atmosphere)

$\Delta G = \Delta G° + 4.575\ T \log p_{CO_2}$ [atm]

$\log p_{CO_2}$ (torr) $= 13.15 - 3.09\ (10^4/T)$ (Figure 25.)

REACTION II

$$2SiC + SiO_2 \rightarrow 3Si + 2CO$$

$\Delta G° = 199700 - 92.0T = 43300$ (calories) at 1 atm., 1700K.

(reaction does not proceed to the right at one atmosphere)

$\Delta G = \Delta G° + 4.575\ T \log p_{CO}^2$ [atm]

$\log p_{CO}$ (torr) $= 12.94 - 2.18\ (10^4/T)$ (Figure 26.)

REACTION III

$$SiC + SiO_2 \rightarrow SiO + CO + Si$$

$\Delta G° = 181600 - 84.1T = 38630$ (calories) at 1 atm., 1700K

(reaction does not proceed to the right at one atmosphere).

$\Delta G = \Delta G° + 4.575\ T \log (p_{SiO})\ (p_{CO})$

$p_{SiO} = p_{CO} = 1/2 p_t$ (total pressure)

$\Delta G = \Delta G° + 9.15 \log p_t$ [atm] $+ 4.575\ T \log 0.250$

$\log p_t$ (torr) $= 12.38 - 1.98\ (10^4/T)$ (Figure 27.)

REACTION IV

$$SiC + 2SiO_2 \rightarrow 3SiO + CO$$

$\Delta G° = 345100 - 160.3T = 72590$ (calories) at 1 atm., 1700K

(reaction does not proceed to the right at one atmosphere).

$$\Delta G = \Delta G° + 4.575T \log (p_{SiO})^3 (p_{CO})$$

$$p_{SiO} = 3\, p_{CO} \quad ; \quad p_t \text{ (total pressure)} = \frac{4}{3}\, p_{SiO}$$

$$\Delta G = \Delta G° + 18.3T \log p_t + 4.575T \log n\ (27/256)$$

$$\log p_t \text{ (torr)} = 11.84 - 1.89\ (10^4/T) \qquad \text{(Figure 28.)}$$

REACTION V

$$SiC + SiO_2 \rightarrow C + 2SiO$$

$\Delta G = 181500 - 80.2T = 45160$ (calories) at 1 atm., 1700K

(reaction does not proceed to the right at one atmosphere)

$$\Delta G = \Delta G° + 4.575T \log p_{SiO}^2$$

$$\log p_t \text{ (torr)} = 11.64 - 1.98\ (10^4/T) \qquad \text{(Figure 29.)}$$

Results

Reactions I - V shown above have been examined. Figures 25 through 29 and the analysis above shows that for four of the five reactions examined (i.e., II - V) a reaction between the silicon carbide coating and the silica crucible will occur in the present working range. However, this reaction can be suppressed by operating at slightly higher pressures. This will introduce complications in heat transfer and will introduce extra costs. Another solution to the above problem is to develop a free-standing crucible. The sintered graded crucibles developed are quite thick and can be eventually made free standing. In the absence of the graphite retainers, the silicon carbide impurities will not be formed in silicon.

Improvement of Heat Extraction through the Crucible

The thermal conductivity of silicon in the molten state is more than twice that in the solid state.[2] This means that the extraction of heat by the heat exchanger is progressively impeded as the interface proceeds. This is further complicated by the fact that the conductivity of the silica crucible drops significantly in the temperature range of seeding and growth cycles.[3] It has been demonstrated[4] at Crystal Systems that a silicon carbide coated graphite plug can be used through a hole at the bottom of a clear silica crucible for more efficient heat transfer. However, the success of this experiment (run 75-C) aided in trying some more experiments. These were carried out to understand the following: (i) use of a graphite plug instead of a silicon carbide coated plug; (ii) the formation of SiC layer on graphite at high temperature; (iii) bonding of the seed to the plug to prevent it from floating in molten silicon; (iv) the formation of a leakproof seal between the plug and the crucible even when the seed is lost.

In an initial experiment, during run 92-C two pieces of silicon single crystal were kept on a graphite piece and a silicon carbide coated graphite piece. The temperature was raised till silicon was molten. The temperature was dropped rapidly. The uncoated graphite piece was bowed which is due to the differential coefficients of expansions. These

samples were examined with an optical microscope. It was found that a silicon carbide layer was present for both samples (Figures 30 and 31). The reaction was not severe to cause disintegration of the uncoated graphite piece.

In a number of runs (Table III) a graphite plug was used in a sintered graded crucible. It was found that the crucible has to be supported to prevent warpage at the bottom. A tight fit between the graphite plug and silica crucible can be formed at high temperatures which is leakproof to molten silicon. A 2 Kg crack-free ingot was cast using such a technique in run 110-C. In spite of the furnace and heat exchanger temperature profiles being higher than regular runs, it was found that the heat transfer through the plug was more efficient. A polished and etched cross section of run 110-C (Figure 32) shows that no melt back of the seed was attained.

The integrity of the compression fit between the graphite plug and the crucible can be judged from run 111-C. During this run the run was aborted due to crucible failure when nearly all of silicon was in molten state. However, there was no penetration of molten silicon through the joint.

Thus it has been proved that a compression fit can be made with a graphite plug and silica crucible which is leak-proof to molten silicon.

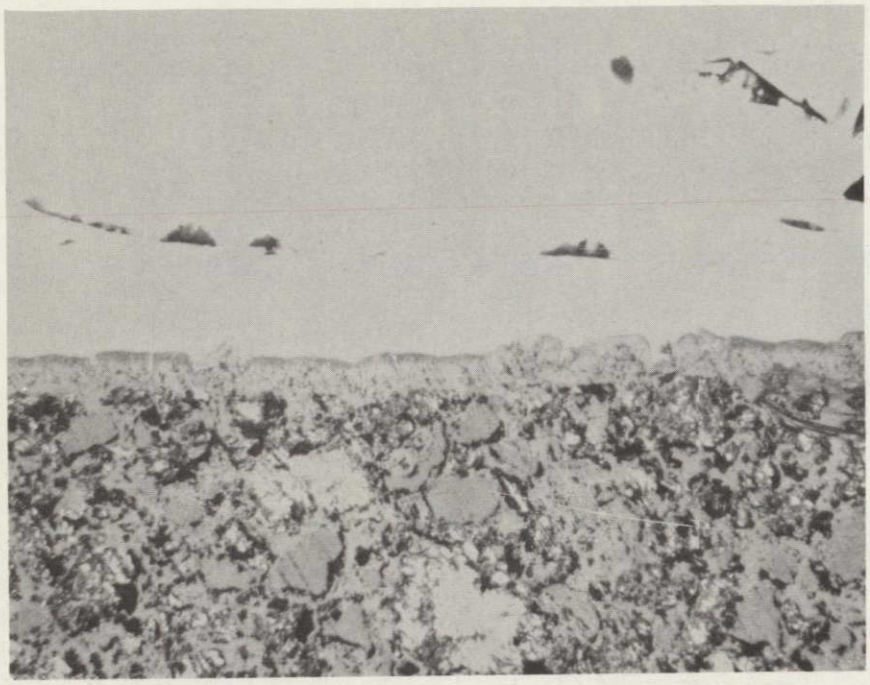

Figure 30. Optical Micrograph (100X) of Silicon on SiC Coated Graphite

Figure 31. Optical Micrograph (100X) of Silicon on Graphite

Figure 32. Polished and Etched Cross-Section of Boule Cast in Run 110-C. The efficient heat transfer through the graphite plug prevented the seed melt-back.

CRYSTAL SLICING

Efforts in silicon slicing were directed towards life tests of 5 mil, 0.125 mm tungsten core, nickel-plated wire with 45 and 30 μm diamonds. Seventy wires were used in a blade pack. Good wafer quality and high yields, 85-97%, were obtained. During these runs (Table VI) studies on some variables were also incorporated.

Life tests using the nickel-plated tungsten core wire were carried out in runs 51-S through 60-S and 62-S through 65-S. The as-received wires after plating measured about 10 mil, 0.254 mm each. The blade pack was used without any dressing before or in between runs. The average thickness of the wafer cut, calculated on the basis of a stack of 20 wafers, was 5.5 mil, 0.140 mm (run 51-S); 6.5 mil, 0.165 mm (run 55-S); and 7.25 mil, 0.184 mm (run 60-S). Initially the average cutting rates were 3.0 mil/min, 0.076 mm/min for run 51-S at 38 gms feed force, but it dropped to 1.13 mil/min, 0.029 mm/min in run 60-S for a feed force of 25 gms. However, in run 57-S when the feed force was 38 gms better cutting rates were obtained. This shows that the feed forces have a strong effect on the cutting rates. It is expected that good cutting rates will be regenerated after suitably dressing

TABLE VI. SILICON SLICING SUMMARY

RUN	PURPOSE	FEED FORCE/BLADE lb	FEED FORCE/BLADE gm	AVERAGE CUTTING RATE mil/min	AVERAGE CUTTING RATE mm/min	WIRE TYPE	REMARKS
51-S	Life test	0.084	38	3.0	0.076	45 μm diamond, Nickel plated, 5 mil, 0.125 mm tungsten core wire	Good wafer quality and cutting rates. 97% yield.
52-S	Life test	0.084	38	2.85	0.072	Same wire.	Good wafer quality and cutting rates. 97% yield.
53-S	Life test	0.084	38	2.36	0.060	Same wire.	Good wafer quality and cutting rates. 97% yield.
54-S	Life test	0.057	26	1.24	0.031	Same wire.	Run terminated after 1.3 in. cutting to leave workpiece intact. 90% yield.
55-S	Life test	0.070	32	1.70	0.043	Same wire.	Good wafer quality. 87% yield.
56-S	Life test	0.070	32	1.46	0.037	Same wire.	Good wafer quality. 85% yield.
57-S	Life test	0.084	38	2.26	0.057	Same wire.	Good wafer quality. 85% yield.
58-S	Life test and effect of shorter stroke --4.5"	0.070	32	1.31	0.033	Same wire.	Good wafer quality. 85% yield.
59-S	Life test and effect of change in stroke--6"	0.070	32	1.45	0.037	Same wire.	Good wafer quality. 85% yield.

TABLE VI. SILICON SLICING SUMMARY (Cont.)

RUN	PURPOSE	FEED FORCE/BLADE lb	gm	AVERAGE CUTTING RATE mil/min	mm/min	WIRE TYPE	REMARKS
60-S	Life test--stroke change midrun. To study effect on wafer surface.	0.056	25	1.13	0.029	Same wire.	Low feed forces used. Wafer characterization in progress.
61-S	Test CSI impregnated wire	N/A		N/A		Copper coated, stainless steel core, diamond impregnated wire.	Run aborted due to binding of wires in cuts.
62-S	Life test	0.074	34	1.64	0.042	45 μm diamond, nickel plated, 5 mil, 0.125 mm tungsten core	80% yield. Good quality wafers.
63-S	Life test	0.075	35	1.93	0.049	Same wire.	78% yield. Poor yield due to roller degradation.
64-S	Life test; new rollers in place	0.075	34	2.04	0.052	Same wire.	Dressing wires and new rollers increased yield to 97%.
65-S	Life test and roller degradation	0.075	34	1.66	0.042	Same wire.	Yield 83%. Rollers were used in run 64-S and show degradation.
66-S	Test new wires 30 μm	0.078	35	2.02	0.051	30 μm diamond, nickel plated, 5 mil, 0.125 mm tungsten core	94% yield. Good wafer quality.
67-S	Life test	0.078	35	1.81	0.046	Same wire.	89% yield. New rollers in place. Lower yield due to wire degradation.

TABLE VI. SILICON SLICING SUMMARY (Cont.)

RUN	PURPOSE	FEED FORCE/BLADE lb	FEED FORCE/BLADE gm	AVERAGE CUTTING RATE mil/min	AVERAGE CUTTING RATE mm/min	WIRE TYPE	REMARKS
68-S	Life test	0.078	35	1.70	0.043	Same wire	78% yield. Good wafer quality. Poor yield due to roller and wire degradation.
69-S	Life test	N/A	-	N/A	-	Same wire	Run aborted for machine modification
70-S	Slice 7.6 cm Ø workpiece	0.066	30	N/A	-	Same wire	Run aborted due to wafer breakage
71-S	Life test	0.066	30	1.90	0.048	Same wire	84% yield. Good quality wafers.

the wires. High wafer yields obtained are indicated in Table VI. The wafers damaged were due to the wires coming together during slicing. Some of the factors contributing to this are roller degradation, misalignment and loss of diamond particles. Analysis to solve this problem is currently in progress.

The usual stroke length in slicing has been 8 inches, 20.3 cm. In run 58-S and 59-S a stroke length of 4.5 inches and 6.0 inches respectively were used. However, the frequency of 108 cycles per minute and a feed force of 0.07 pounds per blade, 32 gms per blade were kept constant. These experimental conditions correspond to a minimum surface feet of 126.3 ft. cycles/min for run 58-S and 169.6 ft. cycles/min for 59-S. Within the limited data taken it appears that the cutting rate increases with increase in surface feet.

In run 60-S the stroke length was changed after cutting part of the way; however, the surface feet was kept constant at 168 by increasing the cycles/min from 80 to 108. No change in cutting rates was observed. This shows that even if the stroke length is changed, it does not affect the cutting rate as long as the surface feet/min is maintained constant. Analysis of the effect of this variable on surface quality of the wafer are currently in progress.

In run 64-S the dressing of wires and new rollers revived good cutting rates and high yields. This blade pack was still cutting well when it was replaced by a 30 μm diamond plated wire blade pack. These wires have been used in runs 66-S through 69-S. It has been proved that the 30 μm diamond can cut efficiently. The 30 μm diamonds are being used to reduce kerf losses. Figure 33 shows a good concentration of diamonds on the longitudinal section of the wire. Figure 34 is a cross-section of this wire. It can be seen that the coating thickness is about half as thick as the core producing an 11 mil, 0.275 mm thick wire. Much of the diamonds are embedded beneath the surface. It was intended to reduce the thickness of the coating to reduce kerf loss.

To slice a 3 inch, 7.6 cm diameter work piece, modification to the multi-blade wafering machine had to be made. This included: (1) Fabrication of a wire support system large enough to span a 7.6 cm work piece; and (2) Fabrication of pivot blocks to rock the work piece about its center.

Run 70-S was undertaken with a 7.6 cm diameter work piece. Extreme vibration in the feed mechanism occurred. This was apparently caused by the added drag forces due to a larger kerf length. The vibration caused 70 to 80% wafer losses. Run 71-S was conducted to verify the cause of the vibration. For this run good quality wafers were sliced with 84% yield.

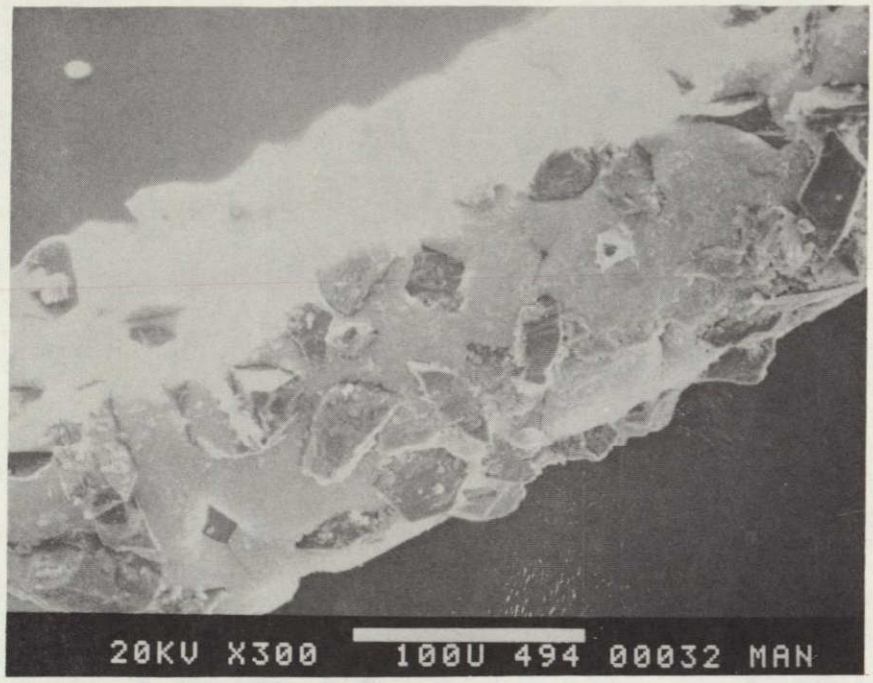

Figure 33. Longitudinal section of diamond plated stainless steel core wire before use in slicing

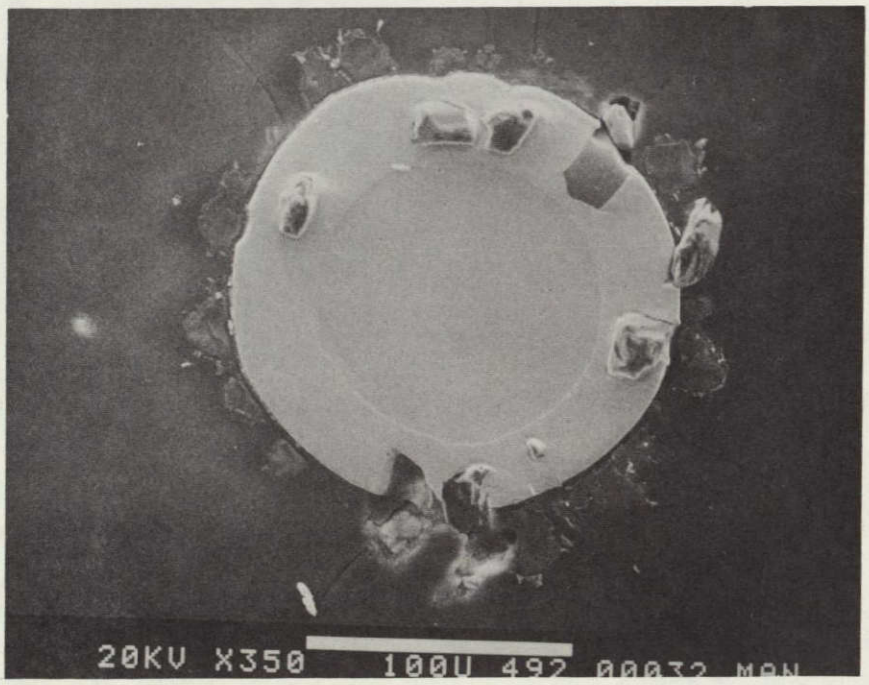

Figure 34. A cross-section of wire in Figure 14.

Examination of the 7.6 cm diameter work piece revealed a non-circular cut profile that was not apparent in 4 x 4 cm work pieces. A non-circular cut profile was caused by crank motion, i.e, lag at end of each stroke. This was undesirable since it did not minimize the contact length between the wire and work piece. The feed mechanism was stiffened and carefully aligned. In addition, the work motion is being replaced by a linear motion.

Wafer Surface Characterization

A sample wafer from a typical run 59-S was examined for surface roughness with a profiliometer. Two scans were taken--one parallel and the other perpendicular to the wire cutting direction. The results are shown in Figure 35. It can be seen that the surface roughness is within ± 0.5 μm.

In an attempt to study the surface damage of the sliced wafers, two slices (one each from run 58-S and 60-S) were butted together and mounted so as to look at the cross-section of the wafers. The wafers were then ground with 15 micron alumina powder followed by diamond paste and finally polished with Syton. Sufficient material was removed so that the final surface should be representative of the "as cut" bulk material and not masked by the grinding operations. The polished

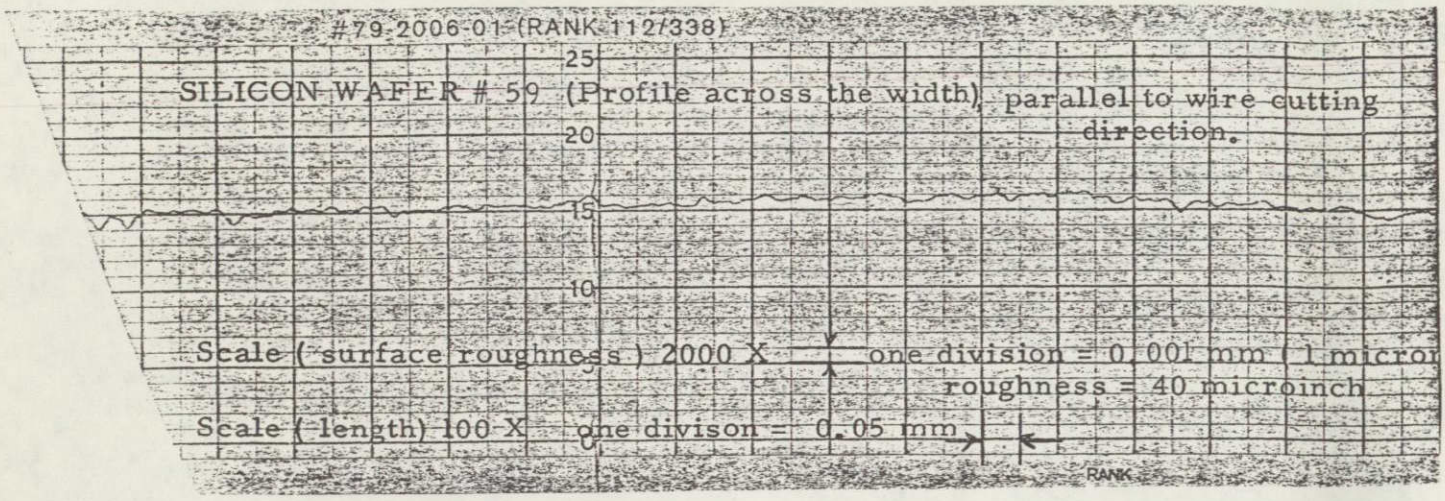

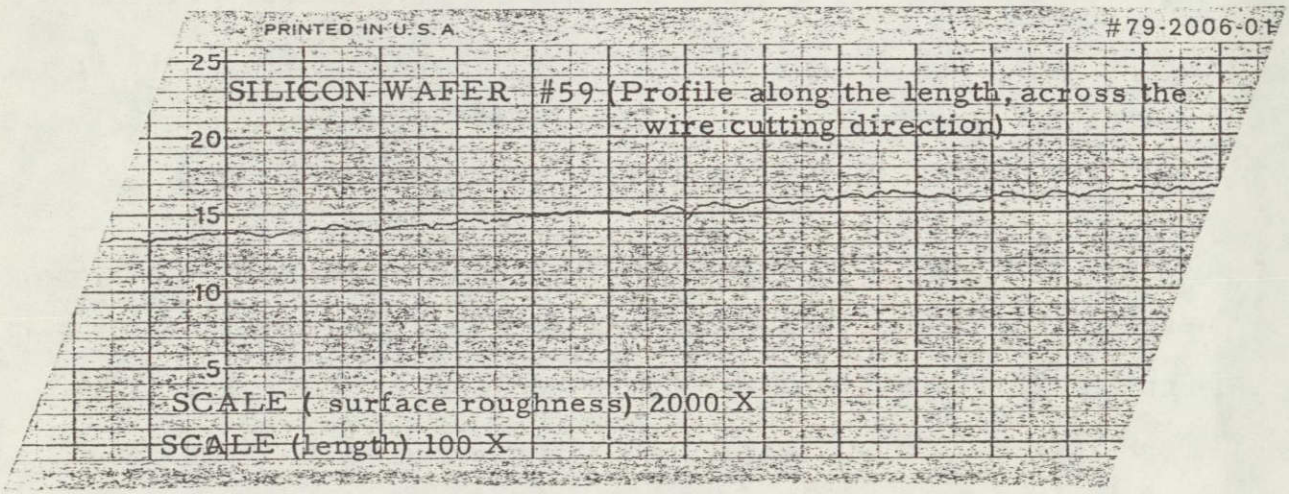

Figure 35. Surface Profiles of a Wafer from Run 59-S.

surfaces were then etched in a Sirtl etch. The depth of damage, as measured by the extent of the fissures into the material, is in the range of up to approximately 3 μm. A SEM photograph of the two wafers is shown in Figure 36 and a magnified view in Figure 37. This depth of damage appears low as compared with other methods of slicing. Steps are underway to prepare a tapered section to investigate the depth of damage further.

Blade Development

So far in the program emphasis has been on a tungsten and stainless steel core material. These were selected so that high forces can be applied to minimize wander of the wires during slicing. In an effort to obtain commercially available coated wire for impregnation, a sample of copper coated 1065 steel core wire was tested for mechanical properties. It was found to have a yield strength in the range of 145,000 to 149,000 psi and a UTS of 184,000 psi. These values are too low, as compared to the tungsten core being used. Another sample examined for mechanical properties was 5.5 mil music wire. It was found to have a yield strength of 420,000 psi and UTS of 515,000 psi. This wire seems to be suitable for the slicing operation. Efforts are on hand to plate this wire so that it can be tested.

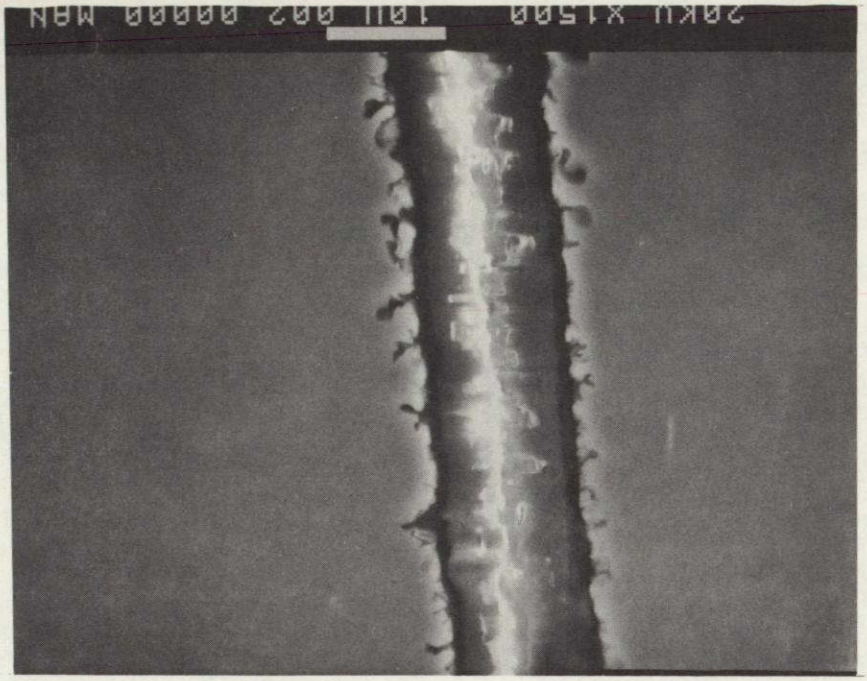

Edge #58 Edge # 60

Figure 36. A SEM photograph of edge of two wafers showing microfissures

Figure 37. A magnified view of the edge of wafer from 58-S.

During the initial periods of the program it was found that a high concentration of diamonds could be plated on stainless steel. There was was a problem with the tungsten core. The plating houses are, in general, not willing to disclose their process because of proprietary nature. However, we were able to work with vendors and achieve satisfactory results with the tungsten core wire. Further, there seems to be a variation in diamond concentration from pack to pack. The life of impregnated wire has been found to be shorter than plated wire because of diamond pull out. It was, therefore, intended to coat a thin layer of plating on the impregnated wire to prevent pull out.

A study was initiated to plate the impregnated wire by electroplating as well as by an electroless process. Both the methods were used to plate three thickness; viz., 0.1 mil, 0.3 mil, and 0.6 mil on commercial as well as Crystal Systems impregnated wires. The electroless plated wires were baked at 175°C, 230°C, and 290°C to study the effect of the temperature of baking. The samples were examined with a SEM. Details of the wires are shown in Table VII. It was found that both the commercial and Crystal Systems wires appeared to clean and plate with no difficulty. The baking treatment on electroless plated wires contracts the plating, thereby holding the diamonds

TABLE VII.

DETAILS OF PLATING OF IMPREGNATED WIRE

WIRE	PROCESS	BAKING TEMPERATURE	PLATING THICKNESS (mil)
Commercial	Electroless	-	0.1
Commercial	Electroless	-	0.3
Commercial	Electroless	-	0.6
Crystal Systems	Electroless	-	0.1
Commercial	Electroless	290°	0.1
Commercial	Electroless	290°	0.3
Commercial	Electroless	290°	0.6
Commercial	Electroplated	-	0.1
Commercial	Electroplated	-	0.3
Commercial	Electroplated	-	0.6
Crystal Systems	Electroplated	-	0.1

stronger. The 0.6 mil thickness plating showed signs of cracking when baked. However, 0.3 mil plating was enough to hold the diamonds (Figure 38). This would also reduce the kerf loss.

The development of impregnation/plating method will be utilized for reducing kerf losses. The diamonds will be impregnated only in the cutting edge by the Crystal Systems process, thereby reducing the costs of blades further.

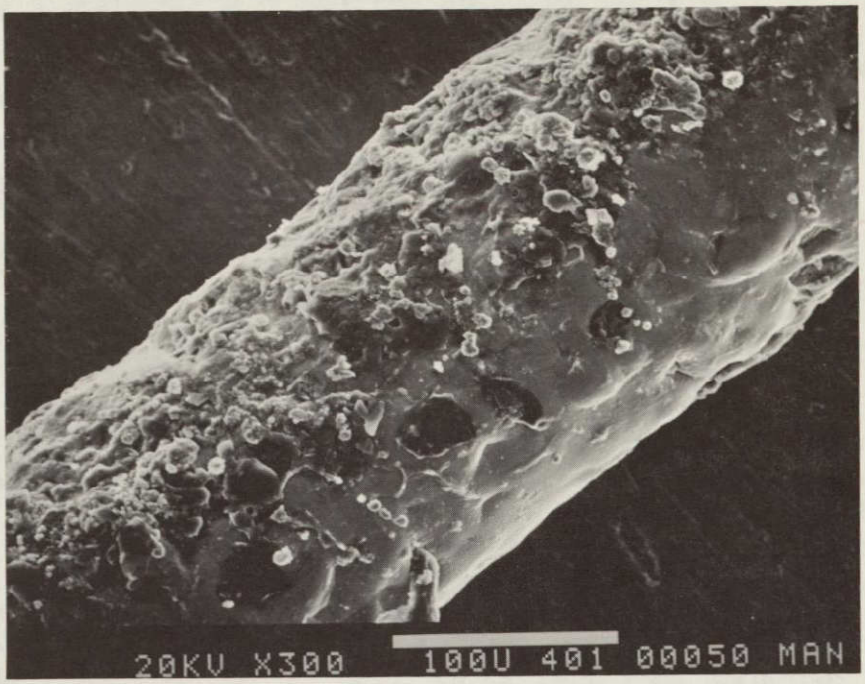

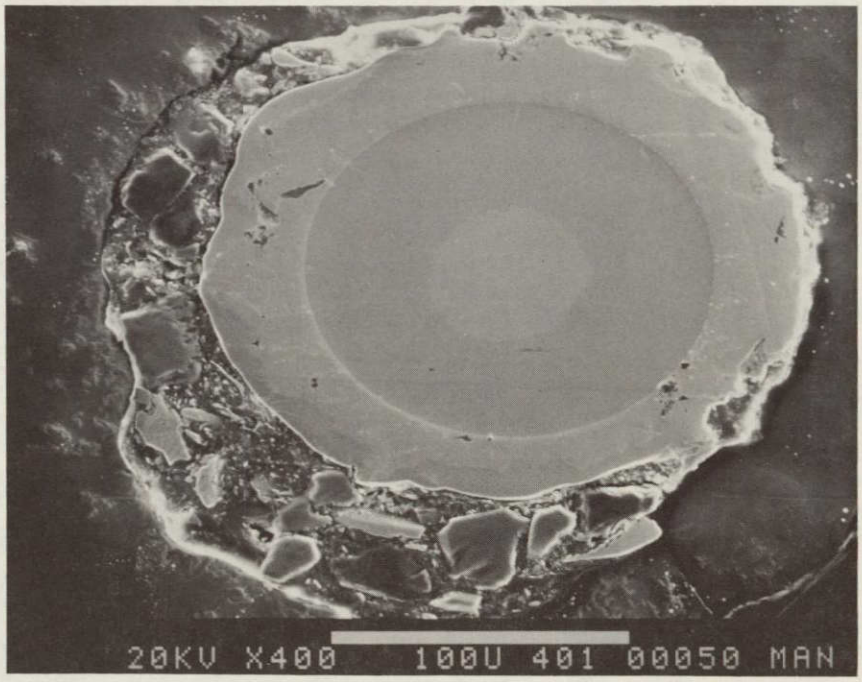

Figure 38. Commercial electroless plated (0.3 mil) wire after 290° bake.

PROJECTED ADD-ON COST ANALYSIS FOR PRODUCING SILICON WAFERS

Ingot Casting

Assumptions:

(1) The plant is based upon producing silicon by the Heat Exchanger Method. The size of the ingot cast is 30 cm X 30 cm X 30 cm.

(2) A 100% yield is obtained, no loss due to grinding or cropping.

(3) No profit.

(4) Cost of a furnace is $75,000. A linear depreciation schedule is assumed[5] based on 10-year life, 52-week at 6 days continuous operation and 83% utilization.

(5) Wages are assumed at $4.50/hr and 4 units/operator basis[5].

(6) Crucible is an expendable item at a cost of $85 each.

(7) Power consumption[5] is based on 10 KW furnace @ 2.5 ¢/KWh.

(8) A $20 per run miscellaneous cost is included for furnace parts, Helium gas, etc.

Ingot Slicing

Assumptions:

(1) Slicing is carried out using a fixed diamond abrasive wire blade.

(2) The 30 cm X 30 cm X 30 cm boule cast will be sectioned into 9 ingots of 30 cm X 10 cm X 10 cm size.

(3) The band-saw sectioning and grinding to exact size is done in 8 hours/boule by equipment costing $40,000. It is used 8 hours/day, 6 days/week, 52 weeks/year and 83% utilization. Linear depreciation schedule is assumed with 15 year life. Wages are assumed at $4.50/hour and 1 unit/operator.

(4) 64 blades/inch are mounted in the blade pack for slicing.

(5) 100% yield, no loss due to breakage of wafers.

(6) Cost of slicer is $30,000. A linear depreciation schedule is assumed based on 10 year life, 52 weeks at 6 days/week continuous operation and 83% utilization.

(7) Wages are assumed at $4.50/hour and 8 slicers/operator basis.

(8) One blade pack cuts through 9 ingots of 30 cm X 10 cm X 10 cm size at a cost of plating of $50/blade pack.

(9) Slicing is at 0.1 mm/minute.

(10) No profit.

(11) A miscellaneous cost of $20 per boule sliced is added for slicer parts, setup epoxy, etc.

1 boule will produce $\frac{30}{100} \times \frac{30}{100} \times 30 \times \frac{64}{2.54} = 68.03$ sq. m of silicon wafer.

Depreciation/boule for sectioning and grinding

$$= \frac{40,000 \times 8}{15 \times 52 \times 6 \times 8 \times 0.83}$$

$$= \$10.30$$

Labor & Overhead/boule for sectioning and grinding

$$= \frac{2.5 \times 4.50 \times 8}{1}$$

$$= \$90.00$$

Total Add-on cost of sectioning and grinding = \$10.30 + \$90.00

= \$100.30

Time to slice 1 ingot (30 cm X 10 cm X 10 cm) at 0.1 mm/minute $= \frac{10}{0.1} \times \frac{10}{60} = 16.67$ Hrs.

Set-up time = 1.33 Hrs.

Time to slice/boule = (16.67 + 1.33) X 9

= 162 Hrs.

Depreciation/boule $= \frac{30,000 \times 162}{10 \times 52 \times 6 \times 24 \times 0.83}$

= \$78.20

Labor & Overhead/boule $= \frac{2.5 \times 4.50 \times 162}{8}$

= \$227.81

Cost of wire and diamond[1] = \$ 0.012/sq m of silicon sliced

= \$ 0.82/boule

Cost of plating = \$ 50.00

Misc. Costs = \$ 20.00

Total Add-on Cost for Slicing/boule

= \$78.20 + \$227.81 + 0.82 + \$50 + \$20 = \$376.83

Total Add-on Cost of Casting, Sectioning and

Slicing/boule = \$309.92 + \$100.30 + \$376.83 = \$787.05

Total Add-on Cost of Casting, Sectioning and

Slicing/sq. m = \$4.56 + \$1.47 + \$5.54 = \$11.57

CONCLUSIONS

1. A graded silica crucible is necessary to cast sound ingots without the problem of penetration of silicon during the molten stage. Different types of graded crucibles have yielded crackfree boules. Ingots as large as 3.3 Kg have been cast.

2. Thermodynamic analysis indicates that silicon carbide is formed predominately by the reaction of carbon monoxide and silicon:

$$CO + 2\ Si \longrightarrow SiC + SiO$$

3. The retainers even if coated with silicon carbide will not impede the evolution of CO under the experimental working range of pressure and temperature.

4. Experimental evidence confirms that in the absence of graphite retainers no silicon carbide is formed.

5. Solar cells with conversion efficiencies greater than 9% (AM1) have been fabricated from silicon cast by the Heat Exchanger Method (HEM). This material is believed to have a high impurity content.

6. Thin silicon wafers, 5.5 to 7.25 mils, 0.140 to 0.184 mm thick can be sliced with yields of 85-97% at the rate of 64 wafers per inch. Both 45 μm and 30 μm diamonds have yielded

good cutting rates.

7. The surface roughness of the wafers sliced is within ± 0.5 μm with surface damage as measured by the extent of microfissures of 3 μm.

8. Kerf losses can be reduced by using impregnated wire. This wire has to be plated with 0.3 mil nickel coating to prevent diamond pull-out.

9. A projected cost analysis using the HEM method of crystal casting and fixed diamond abrasive method of slicing has shown that the add-on cost of casting and slicing will be $11.57 per square meter of silicon sliced.

REFERENCES

1. F. Schmid and C. P. Khattak, "Heat Exchanger-Ingot Casting/Slicing Process," ERDA/JPL 954373, Crystal Systems, Inc., Quarterly Technical Progress Report No. 7, July 1977.

2. Yu. M. Shashkov and V. P. Grishin, Trans. Soviet Phys.--Solid State 8, 447 (1966).

3. R. W. Powell, C. Y. Ho and P. E. Liley, "Thermal Conductivity of Selected Materials," Natl. Bur. Stands. NBS-8, Category 5, 99 (1966).

4. F. Schmid and C. P. Khattak, "Heat Exchanger-Ingot Casting/Slicing Process," ERDA/JPL 954373, Crystal Systems, Inc., Quarterly Technical Progress Report No. 7, July 1977.

5. K. M. Koliwad, M. H. Leipold, G. D. Cumming, and T. G. Digges, Jr., "Economic Analysis of the Cost Silicon Sheet Produced from Czochralski Grown Material," IEEE Photovoltaic Specialists Conference, Baton Rouge, LA, 1976.

SCHEDULE OF MILESTONES: INGOT CASTING

ITEM	DESCRIPTION
1	Modify instrumentation
2	
3	Develop crucible/coating com.
4	
5	Develop max. growth rate
6	
7	Program & Design Review
8	
9	Characterization
10	
11	Determine actual growth rate
12	
13	Growth rate function of h.e.
14	
15	Growth rate function of crucible
16	
17	Monitor interface position
18	
19	Growth rate function of orienta.
20	
21	Growth rate function of diameter
22	
23	Draft final report
24	
25	
26	
27	
28	
29	
30	
31	
32	
33	
34	
35	

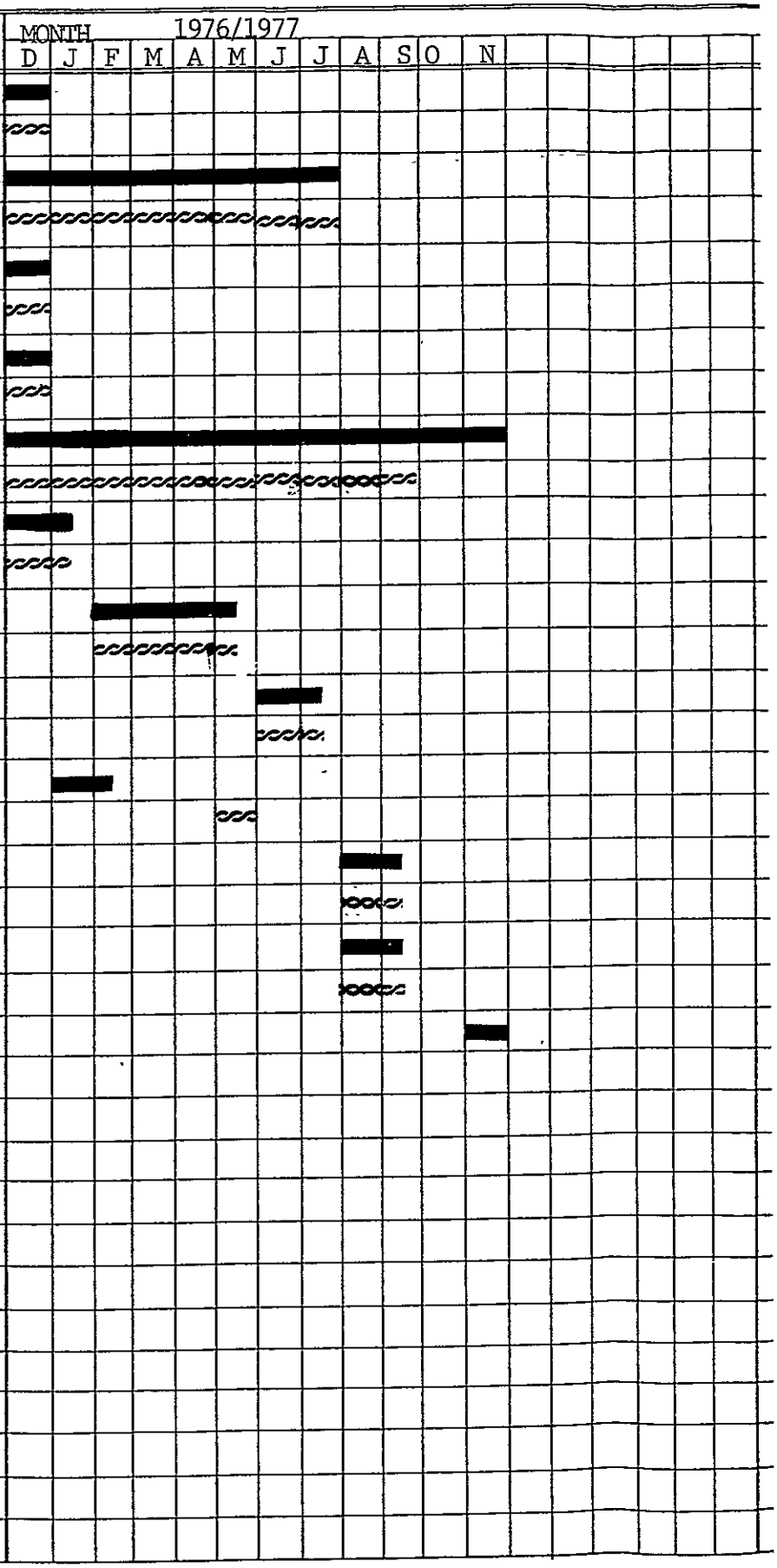

SCHEDULE OF MILESTONES: INGOT SLICING
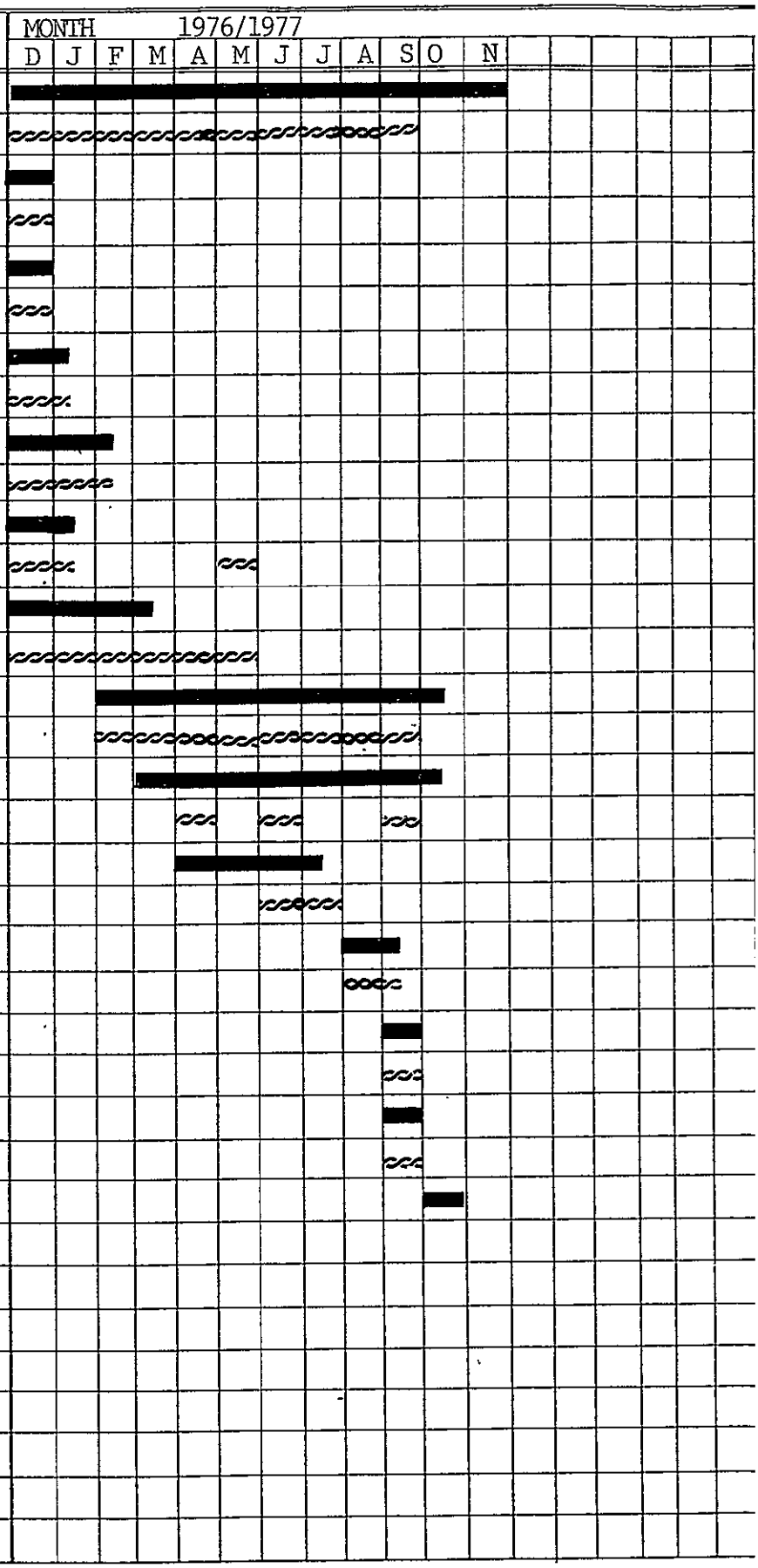
ITEM	DESCRIPTION
1	Characterization
2	
3	Program/Design Review
4	
5	Modify Varian wire support
6	
7	Modify Varian coolant system
8	
9	Diamond-plated tool .005" Ø
10	
11	Diamond-impregnated tool .005" Ø
12	
13	Slicing test -- 4 cm cube
14	
15	Diamond-impregnated tool .003" Ø
16	
17	Diamond-plated tool .003" Ø
18	
19	Slicing tests - 10 cm kerf length
20	
21	Slicing tests - .015 cm wafers
22	
23	Slicing test - 10 cm x 15 cm
24	
25	Slicing test - .015 wafers
26	
27	Draft final report
28	
29	
30	
31	
32	
33	
34	
35